© 2021. Published by The Company of Biologists Ltd | Journal of Cell Science (2021) 134, jcs254920. doi:10.1242/jcs.254920

RESEARCH ARTICLE

The canonical smooth muscle cell marker TAGLN is present in endothelial cells and is involved in angiogenesis

Kiyomi Tsuji-Tamura[1,*,‡], Saori Morino-Koga[1], Shingo Suzuki[2] and Minetaro Ogawa[1,‡]

ABSTRACT

Elongation of vascular endothelial cells (ECs) is an important process in angiogenesis; however, the molecular mechanisms remain unknown. The actin-crosslinking protein TAGLN (transgelin, also known as SM22 or SM22α) is abundantly expressed in smooth muscle cells (SMCs) and is widely used as a canonical marker for this cell type. In the course of studies using mouse embryonic stem cells (ESCs) carrying an *Tagln* promoter-driven fluorescence marker, we noticed activation of the *Tagln* promoter during EC elongation. *Tagln* promoter activation co-occurred with EC elongation in response to vascular endothelial growth factor A (VEGF-A). Inhibition of phosphoinositide 3-kinase (PI3K)–Akt signaling and mTORC1 also induced EC elongation and *Tagln* promoter activation. Human umbilical vein endothelial cells (HUVECs) elongated, activated the *TAGLN* promoter and increased *TAGLN* transcripts in an angiogenesis model. Genetic disruption of *TAGLN* augmented angiogenic behaviors of HUVECs, as did the disruption of *TAGLN2* and *TAGLN3* genes. *Tagln* expression was found in ECs in mouse embryos. Our results identify TAGLN as a putative regulator of angiogenesis whose expression is activated in elongating ECs. This finding provides insight into the cytoskeletal regulation of EC elongation and an improved understanding of the molecular mechanisms underlying the regulation of angiogenesis.

KEY WORDS: TAGLN, Angiogenesis, Endothelial cells, Cell elongation

INTRODUCTION

Cell elongation is a vital activity of vascular endothelial cells (ECs) involved in angiogenesis (Merks et al., 2006; Qutub and Popel, 2009; for reviews see Conway et al., 2001; De Bock et al., 2013; Tsuji-Tamura and Ogawa, 2018b). Vascular endothelial growth factor (VEGF) regulates a wide range of EC activities, including cell elongation (Carmeliet et al., 1996; Ferrara et al., 1996; Geudens and Gerhardt, 2011). Lateral mesodermal cells derived from differentiating embryonic stem cells (ESCs) generate EC colonies when cultured on an OP9 stromal cell layer (Hirashima et al., 1999). VEGF stimulation induces elongation of these ESC-derived ECs, providing an excellent experimental model of ECs undergoing angiogenesis (Hirashima et al., 1999; for reviews, see Tsuji-Tamura and Ogawa, 2018b; Tsuji-Tamura et al., 2011). Various signaling pathways can also induce EC elongation. We previously reported that transforming growth factor (TGF)-β signaling, phosphatidylinositol 3-kinase (PI3K)–Akt and forkhead box O1 (FOXO1) signaling, mammalian target of rapamycin (mTOR) signaling, and glycine signaling induce EC elongation and angiogenesis in coordination with VEGF (Furuyama et al., 2004; Matsukawa et al., 2009; Park et al., 2009; Tsuji-Tamura and Ogawa, 2016, 2018a; Tsuji-Tamura et al., 2020a,b; for reviews, see Tsuji-Tamura and Ogawa, 2018b; Tsuji-Tamura et al., 2011). Some progress has thus been made in the identification of signaling molecules and transcription factors that govern EC elongation. However, the molecular basis of cell elongation itself is poorly understood. It is necessary to identify key molecules that are transcriptionally activated by angiogenic signaling and involved in the regulation of cell morphology.

TAGLN (transgelin, also known as SM22 or SM22α) is widely accepted as a canonical marker of smooth muscle cells (SMCs) (Li et al., 1996; Lees-Miller et al., 1987; Amano et al., 1996). In the course of our previous live-cell imaging study using mouse ESCs that express a fluorescence marker under the control of the *Tagln* promoter (Tsuji-Tamura and Ogawa, 2016), we unexpectedly noticed the activation of *Tagln* promoter not only in ESC-derived SMCs but also in elongated ECs, albeit faintly, in the presence of angiogenic stimuli. TAGLN is known to crosslink actin filaments and bind to actin stress fibers in mesenchymal cells (Shapland et al., 1993). *Tagln* expression is transcriptionally induced when mesenchymal cells come into contact with a culture substrate, enabling cell spreading (Shapland et al., 1988). Furthermore, human umbilical vein endothelial cells (HUVECs) augment *TAGLN* expression upon cell elongation induced by mechanical strain (Cevallos et al., 2006).

In this study, we aimed to test the hypothesis that the *Tagln* gene is activated in angiogenic ECs undergoing morphological changes and plays a role in angiogenesis. We demonstrate promoter activation and induction of expression for *Tagln* in mouse ESC-derived ECs and for *TAGLN* in HUVECs during cell elongation. Expression of the *Tagln* gene was also confirmed in ECs in mouse embryos. Genetic disruption of *TAGLN* isoforms augmented the sprouting behavior of HUVECs. Our observations suggest that TAGLN is expressed in elongating ECs and is involved in the regulation of angiogenesis.

RESULTS

The *Tagln* promoter is activated in ESC-derived SMCs

Previous reports have shown that KDR-positive (KDR^+) mesodermal cells derived from ESCs can differentiate into both ECs and SMCs (Park et al., 2009; Tsuji-Tamura et al., 2011; Yamashita et al., 2000). F10-EGFP/Tagln-DsRed.T4 ESCs (Tsuji-Tamura and Ogawa, 2016) express EGFP and DsRed.T4

[1]Department of Cell Differentiation, Institute of Molecular Embryology and Genetics, Kumamoto University, 2-2-1 Honjo, Kumamoto 860-0811, Japan. [2]Support Section for Education and Research, Faculty of Dental Medicine, Hokkaido University, Kita 13, Nishi 7, Kita-ku, Sapporo 060-8586, Japan.
*Present address: Oral Biochemistry and Molecular Biology, Department of Oral Health Science, Faculty of Dental Medicine and Graduate School of Dental Medicine, Hokkaido University, Kita 13, Nishi 7, Kita-ku, Sapporo 060-8586, Japan.

‡Authors for correspondence (ktamuratsuji@den.hokudai.ac.jp; ogawamin@kumamoto-u.ac.jp)

K.T., 0000-0002-0961-5402

Handling Editor: Kathleen Green
Received 25 September 2020; Accepted 30 June 2021

Journal of Cell Science (2021) 134, jcs254920. doi:10.1242/jcs.254920

fluorescent proteins under the control of an EC-specific transcriptional enhancer of the *Mef2c* gene (F10 enhancer; De Val et al., 2008) and the 440 bp promoter region of the *Tagln* gene (GenBank accession NC_000075.7, bases 45847197–45847636), respectively. The ESCs were cultured on an OP9 stromal cell layer for 3.5 days to induce differentiation of KDR$^+$ mesodermal cells, which were purified using fluorescence-activated cell sorting (FACS; Fig. 1A,B). KDR$^+$ cells differentiated into EGFP-positive DsRed.T4-negative (EGFP$^+$ DsRed.T4$^-$) cells and EGFP$^-$ DsRed.T4$^+$ cells when re-cultured on an OP9 cell layer for 7 days (Fig. 1A,B). KDR$^-$ EGFP$^-$ DsRed.T4$^+$ cells were purified using FACS and further cultured on a gelatin-coated plate for 2 days

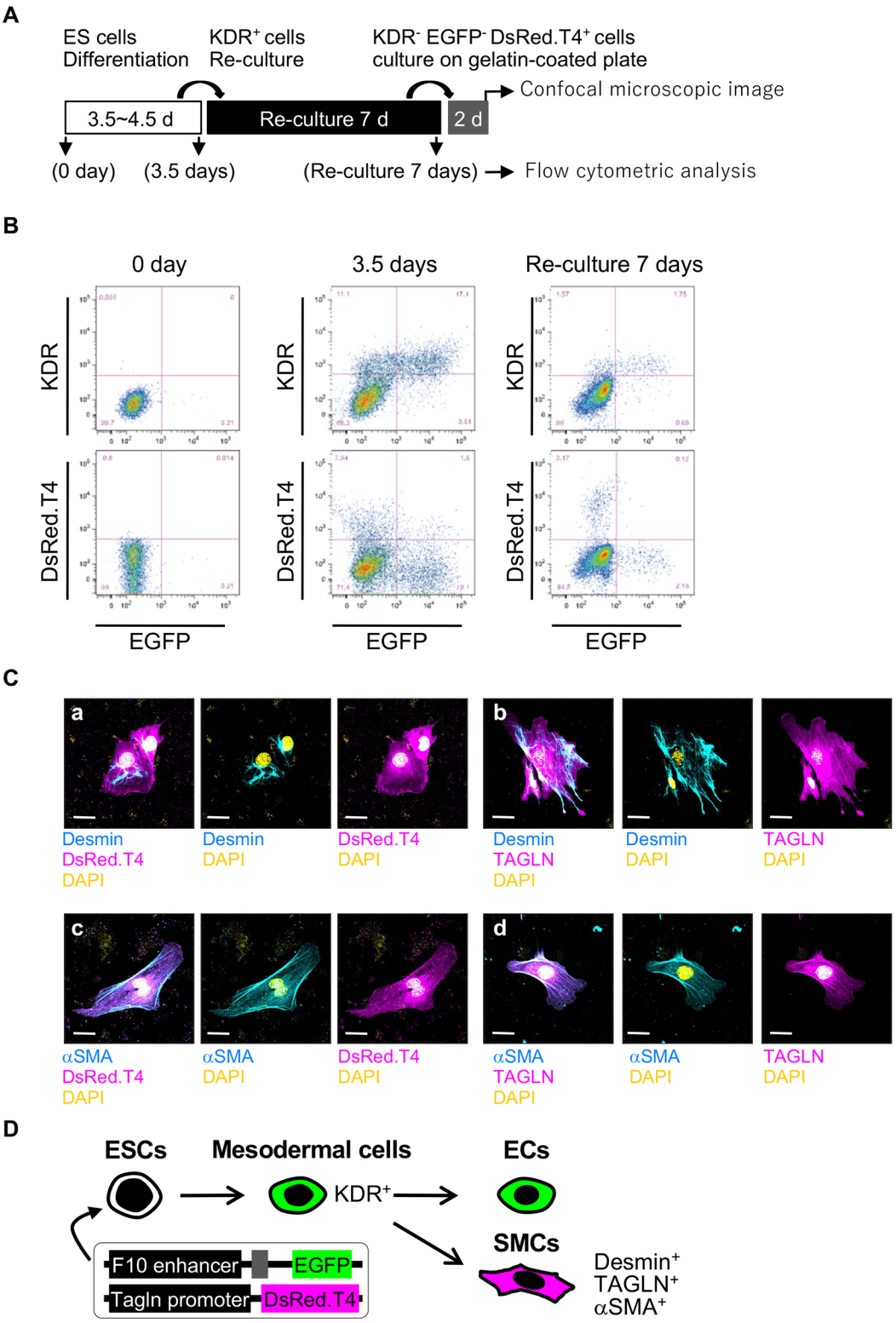

Fig. 1. See next page for legend.

Journal of Cell Science (2021) 134, jcs254920. doi:10.1242/jcs.254920

Fig. 1. The *Tagln* promoter is activated in SMCs derived from ESCs. F10-EGFP/Tagln-DsRed.T4 ESCs were cultured on an OP9 cell layer for 3.5–4.5 days to induce KDR$^+$ mesodermal cells. KDR$^+$ cells were purified using FACS and re-cultured on an OP9 cell layer for 7 days to induce SMCs. KDR$^-$ EGFP$^-$ DsRed.T4$^+$ SMCs were purified using FACS and cultured on gelatin-coated plates for 2 days, followed by immunostaining. (A) Experimental design for SMC and EC induction from ESCs. (B) FACS analyses of KDR, EGFP and DsRed.T4 expression in undifferentiated ESCs on day 0, differentiated cells on day 3.5 of ESC culture and differentiated cells on day 7 of KDR$^+$ cell culture. The lines in each plot indicate the gated population. Similar results were obtained for three independent clones. (C) Immunostaining of SMCs. Multichannel *z*-stack confocal images were merged in maximum intensity projections. Panel a shows desmin (cyan), DsRed.T4 (magenta) and DAPI (yellow). Panel b shows desmin (cyan), TAGLN (ab14106, Abcam; magenta) and DAPI (yellow). Panel c shows αSMA (cyan), DsRed.T4 (magenta) and DAPI (yellow). Panel d shows αSMA (cyan), TAGLN (ab14106, Abcam; magenta) and DAPI (yellow). Scale bars: 20 µm. Similar results were obtained in three independent clones. (D) A schematic model for activation of the F10 enhancer and *Tagln* promoter during differentiation of ECs and SMCs from F10-EGFP/Tagln-DsRed.T4 ESCs. The F10 enhancer is activated in ESC-derived KDR$^+$ mesodermal cells, which are the common precursor cells of both ECs and SMCs (Tsuji-Tamura et al., 2011), and remains active in the differentiated ECs, but becomes inactive in the differentiated SMCs. The *Tagln* promoter is activated in SMCs, but not ECs cultured in normal differentiation conditions.

(Fig. 1A). KDR$^-$ EGFP$^-$ DsRed.T4$^+$ cells expressed differentiation markers of SMCs, including desmin, TAGLN and αSMA (also known as ACTA2) (Fig. 1C). These observations confirmed the activation of the *Tagln* promoter in SMCs differentiated from the ESC-derived mesodermal cells (Fig. 1D).

ECs activate the *Tagln* promoter in response to VEGF

To examine whether the *Tagln* promoter is activated in elongated ECs, ESC-derived KDR$^+$ cells were cultured on an OP9 cell layer in the presence or absence of exogenous VEGF-A$_{165}$ (referred to hereafter as VEGF) to induce EC colony formation, which was directly examined using fluorescence microscopy. In the absence of exogenous VEGF, 70% of EGFP$^+$ EC colonies were sheet-like (Fig. 2A–C). The sheet-like EC colonies did not express DsRed.T4 (Fig. 2A,C). The rest of the EC colonies were sheet-and-cord-like, and partially contained elongated ECs (Fig. 2A–C). Interestingly, these colonies expressed DsRed.T4, albeit weakly (Fig. 2A,C). The addition of VEGF induced EC elongation and resulted in a shift in the morphology of EC colonies from sheet-like to cord-like (Fig. 2A–C). The cord-like EC colonies clearly expressed DsRed.T4 (Fig. 2A,C). Notably, the addition of VEGF did not affect the proportion of EGFP$^+$ EC colonies and EGFP$^-$ DsRed.T4$^+$ SMC colonies (Fig. 2D).

Confocal microscopy analyses of the immunostained cultures revealed cobblestone-like VE-cadherin (CDH5)$^+$ EGFP$^+$ ECs, which formed sheet-like colonies, in the absence of exogenous VEGF (Fig. 2E,G,H). These ECs did not express DsRed.T4 (Fig. 2E,H), while VE-cadherin$^-$ EGFP$^-$ DsRed.T4$^+$ SMCs were detected in the same culture. In the presence of VEGF, the VE-cadherin$^+$ EGFP$^+$ ECs exhibited a thin and elongated morphology (Fig. 2F–H), which is indicative of the angiogenic response of ECs (Hirashima et al., 1999; Tsuji-Tamura and Ogawa, 2016). As expected, these elongated ECs expressed DsRed.T4 (Fig. 2F,H). Cross-sectional (*x*–*z* and *y*–*z*) images confirmed co-expression of EGFP and DsRed.T4 in the elongated ECs (Fig. 2F, panel c). The elongated ECs did not express desmin (Fig. S1). VE-cadherin$^-$ desmin$^+$ SMCs showed higher levels of DsRed.T4 expression than VE-cadherin$^+$ ECs, regardless of whether exogenous VEGF was present (Fig. S1).

We next cultured ESC-derived KDR$^+$ cells as cell aggregates in type I collagen gel containing VEGF. VE-cadherin$^+$ ECs that sprouted out from cell aggregates showed elongated morphology and expressed DsRed.T4 (Fig. 3A,B). The elongated ECs expressed neither αSMA nor desmin, whereas co-existing SMCs expressed high levels of DsRed.T4, αSMA, and desmin. Furthermore, real-time quantitative PCR analyses showed that *Tagln* mRNA was more abundant in the ESC-derived ECs cultured in the presence of VEGF (Fig. S2). The expressions of *Tagln2* and *Tagln3* remained unaffected in the absence and presence of VEGF (Fig. S2).

These results suggest that VEGF stimulation activates the *Tagln* promoter in ECs.

Activation of the *Tagln* promoter is associated with EC elongation

To investigate the kinetics of the *Tagln* promoter activation in ECs, KDR$^+$ cells were seeded onto an OP9 cell layer and cultured for 2 days in the absence of exogenous VEGF. Cells were then treated with VEGF (0 h) and subjected to a time-lapse analysis for 3 days (72 h) (Fig. 3C). Sheet-like EC colonies, which were revealed by EGFP expression at 0 h, started to change their shape and projected elongated ECs from their periphery after 3–6 h (Fig. 3D). This initial morphological change was accompanied by activated DsRed.T4, and the expression was increasingly augmented in the sprouting ECs within 72 h (Fig. 3D). This result indicated that the *Tagln* promoter was activated synchronously with EC elongation (Fig. 3E).

We next aimed to exclude the possibility that the *Tagln* promoter was artificially activated by strong VEGF signaling and was not necessarily linked to EC elongation. We previously reported that EC elongation is induced even at a low level of VEGF by inhibiting either the PI3K–Akt or mTORC1 signaling pathways (Tsuji-Tamura and Ogawa, 2016). When KDR$^+$ cells were cultured on an OP9 cell layer with PI3K–Akt inhibitors (LY294002 and Akt inhibitor VIII) or mTORC1 inhibitors (everolimus and rapamycin) (Fig. 4A), VE-cadherin$^+$ EGFP$^+$ ECs showed an elongated morphology in the absence of exogenous VEGF (Fig. 4B,C). These elongated ECs expressed DsRed.T4 (Fig. 4B,C). Flow cytometric analyses showed that inhibition of PI3K–Akt signaling or mTORC1, as well as VEGF stimulation, increased the intensity of DsRed.T4 fluorescence in the VE-cadherin$^+$ EGFP$^+$ ECs (Fig. 5). These results suggest that the *Tagln* promoter activation is associated with EC elongation, regardless of the inducing signal.

The *TAGLN* promoter is activated in primary ECs

HUVECs change their form according to culture conditions. We observed an amoeboid cell shape when HUVECs were cultured on a gelatin-coated surface (gelatin-coated culture), while the cells became thin and elongated when cultured between two layers of type I collagen gel (3D sandwich culture) (Fig. 6A). The mammalian *TAGLN* family has three isoforms: *TAGLN*, *TAGLN2* (also known as *transgelin 2*) and *TAGLN3* (also known as *transgelin 3*) (Kim et al., 2018), all of which are known to interact with the actin cytoskeleton (Fu et al., 2000; Gimona et al., 2003). HUVECs expressed three isoforms of *TAGLN* (Fig. 6B). Real-time quantitative PCR analyses showed that the expression level of *TAGLN* transcript was higher in 3D sandwich culture than in gelatin-coated culture (Fig. 6C). The expression levels of *TAGLN2* and *TAGLN3* were unaffected in these cultures (Fig. 6C). Luciferase reporter analyses confirmed the activity of the *TAGLN* promoter in both gelatin-coated culture and 3D sandwich culture (Fig. 6D). The *TAGLN* promoter activity was significantly higher in 3D sandwich

Journal of Cell Science (2021) 134, jcs254920. doi:10.1242/jcs.254920

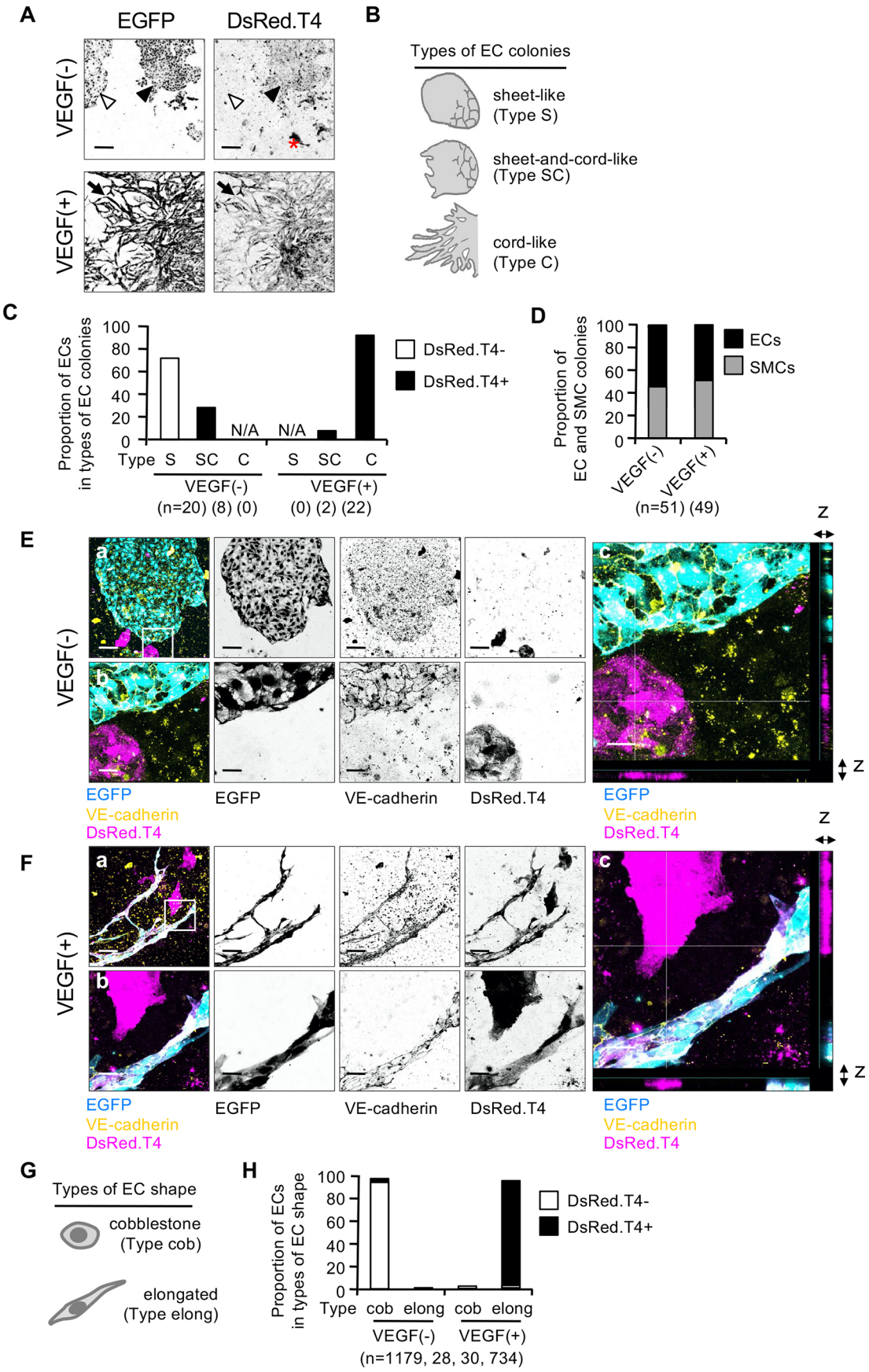

Fig. 2. See next page for legend.

Journal of Cell Science (2021) 134, jcs254920. doi:10.1242/jcs.254920

Fig. 2. The *Tagln* promoter is activated in ECs stimulated with VEGF. KDR$^+$ cells induced from F10-EGFP/Tagln-DsRed.T4 ESCs were cultured on an OP9 cell layer for 4 days with or without the addition of VEGF (10 ng/ml). (A) Images of EGFP and DsRed.T4 fluorescence shown as inverted grayscale images. White arrowheads indicate a sheet-like EC colony expressing EGFP but not DsRed.T4. Black arrowheads indicate a sheet-and-cord-like EC colony expressing both EGFP and DsRed.T4. Black arrows indicate a cord-like EC colony expressing both EGFP and DsRed.T4. The red asterisk indicates an SMC colony expressing only DsRed.T4. Scale bars: 200 µm. (B) Schematic illustration of EC colonies. ESC-derived ECs form three types of colonies: round sheet-like colonies (sheet-like, type S), sheet-like colonies partially containing cord-like cells (sheet-and-cord-like, type SC), and long cord-like colonies (cord-like, type C). (C) EC colonies were categorized based on the colony types described in B and scored as either DsRed.T4$^+$ or DsRed.T4$^-$. The proportion (%) of DsRed.T4-negative and -positive colonies in the three types of EC colonies is shown (N/A, not applicable). The total number of EC colonies in each colony type from two independent experiments using different clones is indicated in the brackets. (D) The proportion (%) of EC and SMC colonies in the presence or absence of VEGF. The total number of colonies examined is indicated in the brackets. Similar results were obtained in two independent experiments using different clones. (E,F) Confocal images of cultures after fixation and immunostaining. Multiple and individual channels are shown as merged and inverted grayscale images, respectively. Images show EGFP (cyan), VE-cadherin (yellow) and DsRed.T4 (magenta) immunostaining of cells cultured in the absence (E) or presence (F) of exogenous VEGF. Panels b and c show higher magnifications of the boxed area in panel a. White lines in panel c indicate sections shown in *z*-axis reconstructions (double-headed arrows). Scale bars: 100 µm (a), 20 µm (b and c). Similar results were obtained in three independent experiments using two clones. (G) Schematic illustration of EC shape. There are two types of EC shape: round and cobblestone-like ECs (cobblestone, type cob), and thin and elongated ECs (elongated, type elong). (H) ECs were categorized into the two types of EC shape described in G and scored as either DsRed.T4$^+$ or DsRedT4$^-$. The proportion (%) of DsRed.T4$^-$ and DsRed.T4$^+$ ECs with the two types of EC shape are shown. The total number of ECs of each shape for the two VEGF treatments, observed across three independent experiments using different clones, is indicated in the brackets.

culture compared to the activity in gelatin-coated culture (Fig. 6D). The significant activities of the *TAGLN2* and *TAGLN3* promoters were similarly detected in both gelatin-coated culture and 3D sandwich culture (Fig. 6D). Western blotting analysis using antibodies against the TAGLN protein (ab14106, Abcam) showed increased signal intensity in 3D sandwich culture compared to the levels in gelatin-coated culture (Fig. 6E).

When HUVECs were cultured as spheroids in type I collagen gel, bundles of elongated cells sprouted out from the spheroids (Fig. 6F). The sprouting cells expressed TAGLN protein, as detected using immunofluorescence staining (Fig. 6F). TAGLN protein partially colocalized with actin filaments, especially at the periphery of the cells (Fig. 6F). These results suggest that three *TAGLN* isoforms are expressed in primary ECs. The expression of *TAGLN* may be induced in elongated ECs in response to angiogenic stimuli, whereas *TAGLN2* and *TAGLN3* appear to be constitutively expressed in ECs.

Single and triple knockout of *TAGLN* isoforms causes excessive cord-like structure formation

We next investigated whether TAGLN plays any roles in the regulation of EC morphology by using HUVECs. We generated HUVECs lacking each isoform (single knockout, SKO) or all three isoforms (triple knockout, TKO) using the CRISPR/Cas9 system (Fig. S3A,B). These gene knockout cells did not show compensatory expression of the other isoforms (Fig. S3C). Western blotting analysis using antibodies against either the C-terminal region (ab14106, Abcam) or the near N-terminal region (HPA019467, Sigma-Aldrich) of the TAGLN protein showed a decrease or disappearance of signal intensity in SKO cells regardless of which isoform was deleted (Fig. 7A). As the signal was absent in TKO cells (Fig. 7A), the anti-TAGLN antibodies used in this study are suggested to recognize all three isoforms. Although the anti-TAGLN antibodies might not discriminate between isoforms, we refer to the protein expression detected by these antibodies as TAGLN protein expression in this article for the sake of simplicity.

In the 3D sandwich culture of genetically modified HUVECs, TKO cells formed an increased number of cord-like structures compared to parental and SKO cells (Fig. 7B,C). The number of branch points was also higher for TKO cells (Fig. 7D). The cord length increased in both SKO and TKO cells compared to that of parental cells, and TKO cell cord length was significantly higher than that of SKO cells (Fig. 7E). In rescue experiments, expression of the zebrafish *tagln* gene suppressed the augmented cord-like structure formation caused by *TAGLN* TKO (Fig. 7B–E). A scratch-wound assay showed that the migration rate was increased in SKO cells compared with that of parental cells (Fig. S4). The migration of TKO cells was significantly higher than that of SKO cells and was suppressed by expression of the zebrafish *tagln* gene (Fig. S4). Notably, the cell proliferation rate was not altered by the deletion of the *TAGLN* isoforms (Fig. 7F).

Furthermore, we performed transfection of siRNA targeting each *TAGLN* isoform (single knockdown, SKD) or all three isoforms (triple knockdown, TKD) into HUVECs. The mRNA and protein expression levels of each isoform were reduced to low or undetectable levels in SKD or TKD cells, showing that these siRNAs were effective in silencing *TAGLN* isoform expression (Fig. S5A,B). In the 3D sandwich culture, although SKD and TKD of *TAGLN* isoforms did not affect the number of cords (Fig. S5C,D), TKD increased the number of branch points compared with the number formed by control and SKD cells (Fig. S5E). Consistent with our observations of SKO and TKO cells (Fig. 7E), the cord length increased in SKD and TKD cultures compared to that in cultures of control cells, and the length of cords formed by TKO cells was significantly higher than those formed by SKO cells (Fig. S5F).

These results appear to suggest that TAGLN negatively regulates the sprouting behavior of HUVECs. On the other hand, overexpression (up to 67-fold) of mouse *Tagln* in HUVECs did not affect the cord formation (Fig. S5G–K), implying that TAGLN may have more complicated and delicate functions in angiogenesis.

ECs of the developing limb vessels of mouse embryos express TAGLN proteins

We next examined whether ECs in mouse embryos express the *Tagln* isoforms. Reverse transcription (RT)-PCR analyses showed that CD45$^-$ CD31$^+$ VE-cadherin$^+$ KDR$^+$ ECs sorted from whole mouse embryos at embryonic day 10.5 (E10.5) expressed transcripts of the three *Tagln* isoforms (Fig. 8A).

We performed whole-mount immunostaining of the limb vessels of E11.5 mouse embryos, which are not yet covered with SMCs (Ben Shoham et al., 2012). TAGLN proteins were detected in ECs that were marked by the presence of KDR, VE-cadherin or isolectin B4, and by the absence of αSMA (Fig. 8B–D). The specificity of staining was confirmed using an isotype-matched control antibody, which gave no signal (Fig. 8E). SMCs in the dorsal aorta at the same stage showed robust staining of αSMA and TAGLN (Fig. 8B–D).

To further confirm the *Tagln* expression in embryonic ECs, we analyzed two single-cell RNA-seq (scRNA-seq) datasets.

Journal of Cell Science (2021) 134, jcs254920. doi:10.1242/jcs.254920

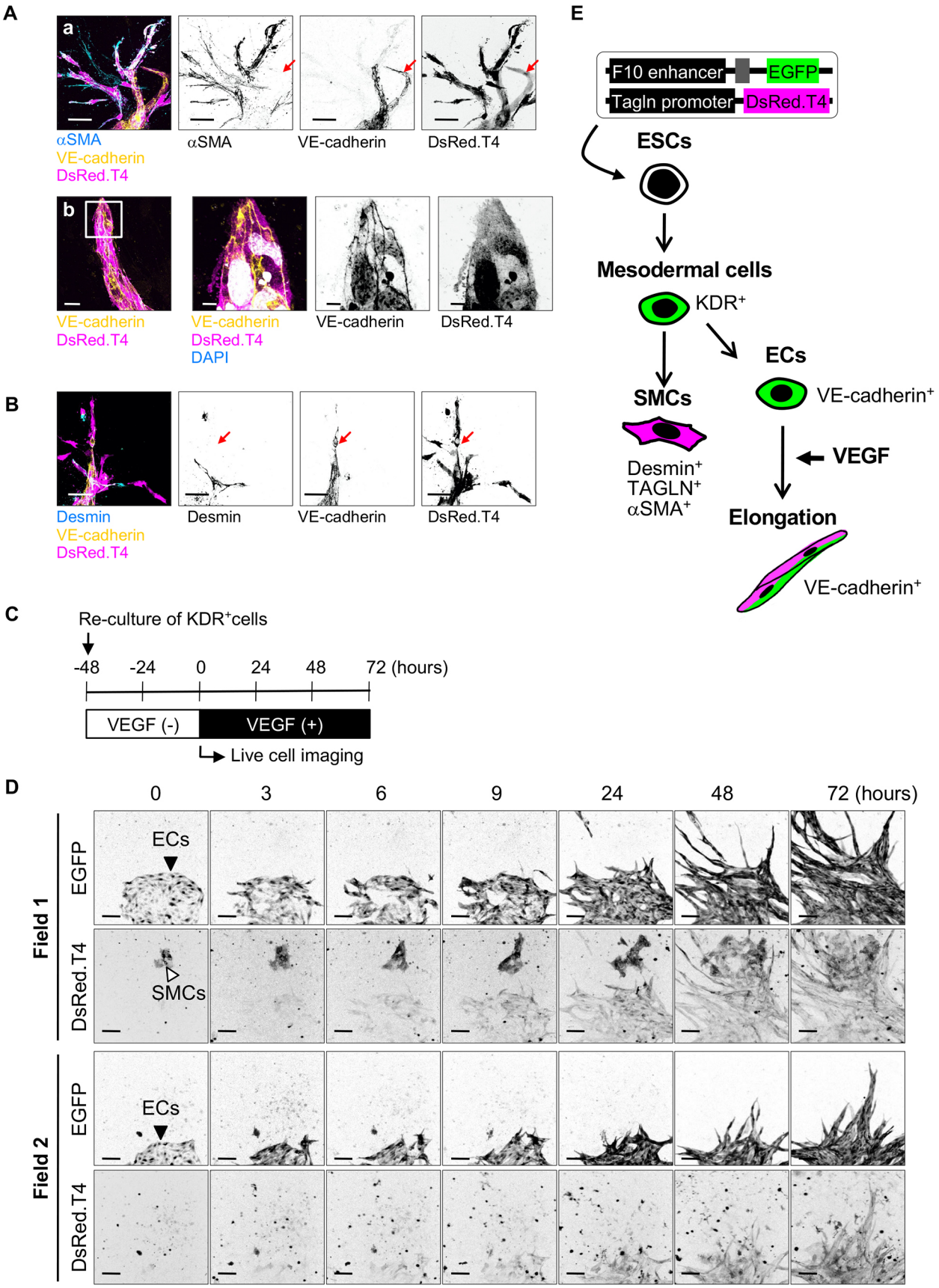

Fig. 3. See next page for legend.

Journal of Cell Science (2021) 134, jcs254920. doi:10.1242/jcs.254920

Fig. 3. The *Tagln* promoter is activated synchronously with EC elongation. (A,B) Aggregations of KDR$^+$ cells derived from F10-EGFP/Tagln-DsRed.T4 ESCs were mounted in type I collagen gel and cultured in the presence of VEGF (10 ng/ml) for 4 days to induce vessel-like structures. (A) Immunostaining of αSMA (cyan), VE-cadherin (yellow) and DsRed.T4 (magenta) is shown in panel a. Red arrows indicate a sprouting EC. Scale bars: 50 µm. Panel b shows close observation of VE-cadherin (yellow), DsRed.T4 (magenta) and DAPI (cyan) staining of ECs. The boxed area in the left-hand image is shown at higher magnification in the images on the right. Scale bars: 20 µm (left), 5 µm (right). (B) Immunostaining of desmin (cyan), VE-cadherin (yellow) and DsRed.T4 (magenta). Red arrows indicate a sprouting EC. Scale bars: 50 µm. Similar results were obtained in three independent experiments using two clones. Single-channel images in A and B are shown in inverted grayscale. (C,D) KDR$^+$ cells induced from F10-EGFP/Tagln-DsRed.T4 ESCs were cultured on an OP9 cell layer in the absence of exogenous VEGF. After 2 days, VEGF (10 ng/ml) was added (defined as 0 h), and the cultures were subjected to time-lapse imaging of EGFP and DsRed.T4 fluorescence. (C) Experimental design for live-cell imaging of *Tagln* promoter activation. (D) Time-lapse images of EGFP (upper panels) and DsRed.T4 (lower panels) fluorescence in two different fields of view, presented as inverted grayscale images. Black arrowheads show EC colonies. A white arrowhead shows an SMC colony. Scale bars: 100 µm. Similar results were obtained in three independent experiments using two clones. (E) A schematic model for activation of the F10 enhancer and the *Tagln* promoter during differentiation and elongation of ECs. ECs differentiated from F10-EGFP/Tagln-DsRed.T4 ESCs are round and cobblestone-like and express only EGFP. ECs treated with angiogenic stimuli, such as VEGF, exhibit elongated cord-like morphology and express DsRed.T4 in addition to EGFP.

Consistent with our observations, a dataset of E10.5 mouse embryonic aortas (Baron et al., 2018) showed that *Tagln*-expressing cells were detected in the EC clusters (Fig. S6). Comparison of *Tagln*-positive and *Tagln*-negative ECs identified 95 genes that were preferentially expressed in *Tagln*-positive ECs (≥1.25-fold change; Table S1). Interestingly, these genes were enriched for morphology-associated gene ontology (GO) terms, such as angiogenesis, blood vessel morphogenesis and tube morphogenesis (Table S2). We further performed scRNA-seq analysis of the aorta–gonad–mesonephros (AGM) region and the fetal liver (FL) of an E10.5 mouse embryo. Our scRNA-seq dataset also showed the presence of *Tagln*-expressing cells in the two EC clusters, which represented arterial and venous ECs (Fig. S7). *Tagln*-positive ECs were more abundant in arterial ECs than in venous ECs (Fig. S7). *Tagln2* was expressed in the whole EC cluster, whereas *Tagln3*-positive cells were barely detected (Fig. S7). The EC clusters hardly expressed the markers of SMC precursors and mature SMCs, excluding *Acta2* (which encodes αSMA protein). The feature plots of total cells showed that the EC clusters were clearly separated from the SMC cluster (Fig. S8), although *Acta2* was expressed in EC clusters (Fig. S7B). Thirty-eight genes were detected as characteristic genes in *Tagln*-positive ECs compared with *Tagln*-negative ECs in the arterial EC cluster (≥1.25-fold change; Table S3), and this set contained five genes in common with the set of highly expressed genes in *Tagln*-positive ECs extracted from the public dataset (Tables S1,S3). These genes were related to 85 GO terms (Table S4), which included eight out of the nine terms obtained from the public dataset (Tables S2,S4). These results suggest that *Tagln* is expressed in ECs of mouse embryos.

DISCUSSION

In this study, we observed *Tagln* expression in mouse ESC-derived ECs and HUVECs undergoing cell elongation in response to angiogenic stimuli. ECs of developing mouse embryos also expressed the *Tagln* gene. Furthermore, knockout or knockdown of the *TAGLN* isoforms (*TAGLN*, *TAGLN2* and *TAGLN3*) in HUVECs resulted in excessive formation of cord-like structures. To the best of our knowledge, this is the first report demonstrating the involvement of TAGLN in the physiological angiogenesis of ECs.

ECs have been reported to transdifferentiate into SMCs under certain conditions; this process is known as endothelial-to-mesenchymal transition (EndMT; for a review see Choi et al., 2020). Cyclic strain induces the expression of TAGLN and αSMA in HUVECs (Cevallos et al., 2006). The prolonged culture of adult bovine aorta ECs results in the expression of TAGLN, αSMA, calponin and smooth muscle myosin heavy chain (Frid et al., 2002). These transdifferentiated cells acquire a flat and enlarged SMC-like morphology. ECs expressing αSMA also occur in developing heart or lung (Hall et al., 2002; Liebner et al., 2004), as well as in pathological changes such as fibrosis (Zeisberg et al., 2007; for a review see Arciniegas et al., 2007). Therefore, the significance of TAGLN expression in ECs must be interpreted carefully, with a distinction between physiological and pathological conditions.

We prefer to avoid the possibility of transdifferentiation for the following reasons. The ESC culture system used in this study recapitulates the developmental process of EC and SMC lineage differentiation from the lateral mesoderm (Yamashita et al., 2000). The ESC-derived ECs elongate in response to VEGF, thus resembling angiogenic sprouting (Hirashima et al., 1999; Tsuji-Tamura et al., 2011). The elongated ECs, which activated the *Tagln* promoter in this study, still retained expression of the EC marker VE-cadherin, while SMC markers such as desmin and αSMA, were not detected. Inhibition of PI3K–Akt or mTORC1 signaling also induced EC elongation and activated the *Tagln* promoter. Furthermore, we detected an increase in *TAGLN* expression in HUVECs that formed elongated cord-like structures under angiogenic culture conditions in the presence of VEGF. In agreement with our observation that ECs in the mouse embryos express *Tagln*, a lineage-tracing study using *Tagln* promoter-driven Cre recombinase has reported marking of ECs of the dorsal aorta in the reporter mouse embryos (Zovein et al., 2008). These observations suggest that *Tagln* expression occurs in the EC lineage under angiogenic conditions, without transdifferentiation into the SMC lineage via an EndMT. This notion might be supported by our scRNA-seq data analysis, suggesting a possible involvement of TAGLN in embryonic ECs undergoing angiogenesis.

Our analysis of two scRNA-seq datasets showed that expression of the *Acta2* gene was enriched in *Tagln*-positive ECs. *Acta2* is predominantly present in SMCs, but has been reported to be expressed in a variety of non-SMC cell types including ECs under certain conditions (Cevallos et al., 2006; Frid et al., 2002; Hautmann et al., 1999; for a review see Owens et al., 2004). The expression pattern of *Acta2* appeared to be similar to that of *Tagln*. Although *Acta2* was not detected in ECs in our other experiments, it cannot be denied that *Acta2* may also be involved in modulating the physiological behavior of ECs.

Tagln-deficient mice do not show any developmental defects (Zhang et al., 2001). Thus, TAGLN appears to be dispensable for normal development, including vascular formation. This could be due to a redundant function of TAGLN isoforms. Indeed, all three *Tagln* isoforms were detected in ESC-derived ECs, cultured HUVECs and ECs isolated from mouse embryos in our experiments, as has also been shown in freshly isolated human umbilical arterial ECs (HUAECs) and HUVECs (NCBI GEO accession GSE43475; Aranguren et al., 2013).

TAGLN has been recognized to influence the dynamics and stabilization of actin (Camoretti-Mercado et al., 1998; Fu et al.,

Journal of Cell Science (2021) 134, jcs254920. doi:10.1242/jcs.254920

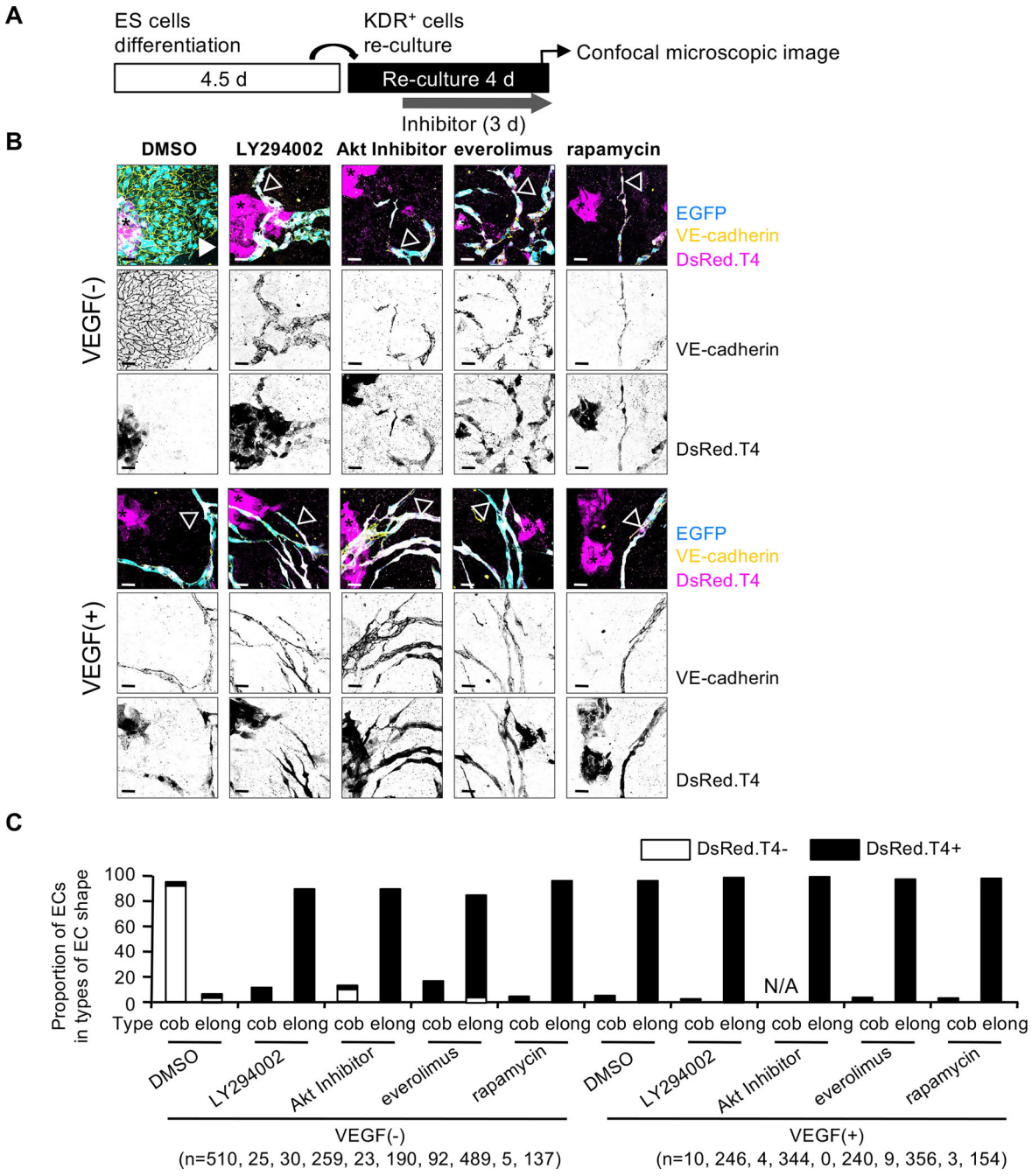

Fig. 4. Activation of the *Tagln* promoter accompanies EC elongation induced by various pathways. KDR$^+$ cells induced from F10-EGFP/Tagln-DsRed.T4 ESCs were cultured on an OP9 cell layer with or without VEGF (10 ng/ml). After 1 day, cells were treated with 5 µM chemical inhibitors (LY294002, Akt inhibitor VIII, everolimus or rapamycin) or DMSO as a vehicle control, and incubated for a further 3 days. Expression of EGFP, VE-cadherin and DsRed.T4 was analyzed using confocal microscopy. (A) Experimental design for ESC differentiation and inhibitor treatment. (B) Confocal images of EGFP (cyan), VE-cadherin (yellow) and DsRed.T4 (magenta). Black asterisks indicate SMC colonies. Filled and unfilled arrowheads indicate a sheet-like EC colony and cord-like ECs, respectively. Single-channel images are shown in inverted grayscale. Scale bars: 50 µm. Similar results were obtained in three independent experiments using two clones. (C) The proportion (%) of DsRed.T4-negative and -positive ECs in the two types of EC shape: cobblestone (type cob) and elongated (type elong). N/A, not applicable. The total number of ECs of each shape for each treatment, examined in three independent experiments using two clones, is indicated in the brackets.

2000; Kim et al., 2018; Lawson et al., 1997; Zeidan et al., 2004; for a review see Assinder et al., 2009), nevertheless, its physiological function remains unclear. We successfully demonstrated that single and triple knockout of the *TAGLN* isoforms in HUVECs promoted migration, but not proliferation, leading to excessive angiogenic cord formation. Similar results were obtained following single or triple knockdown of the *TAGLN* isoforms in HUVECs, thus identifying the TAGLN isoforms as negative regulators of angiogenesis.

The disruption of *TAGLN* promoted cord formation in HUVECs, whereas overexpression of *Tagln* had no effect on this process. Interactions between TAGLN and several factors, including high-mobility group AT-hook 2 (HMGA2), cartilage oligomeric matrix protein (COMP) and poly(ADP-ribose) polymerase 1 (PARP1), have

Journal of Cell Science (2021) 134, jcs254920. doi:10.1242/jcs.254920

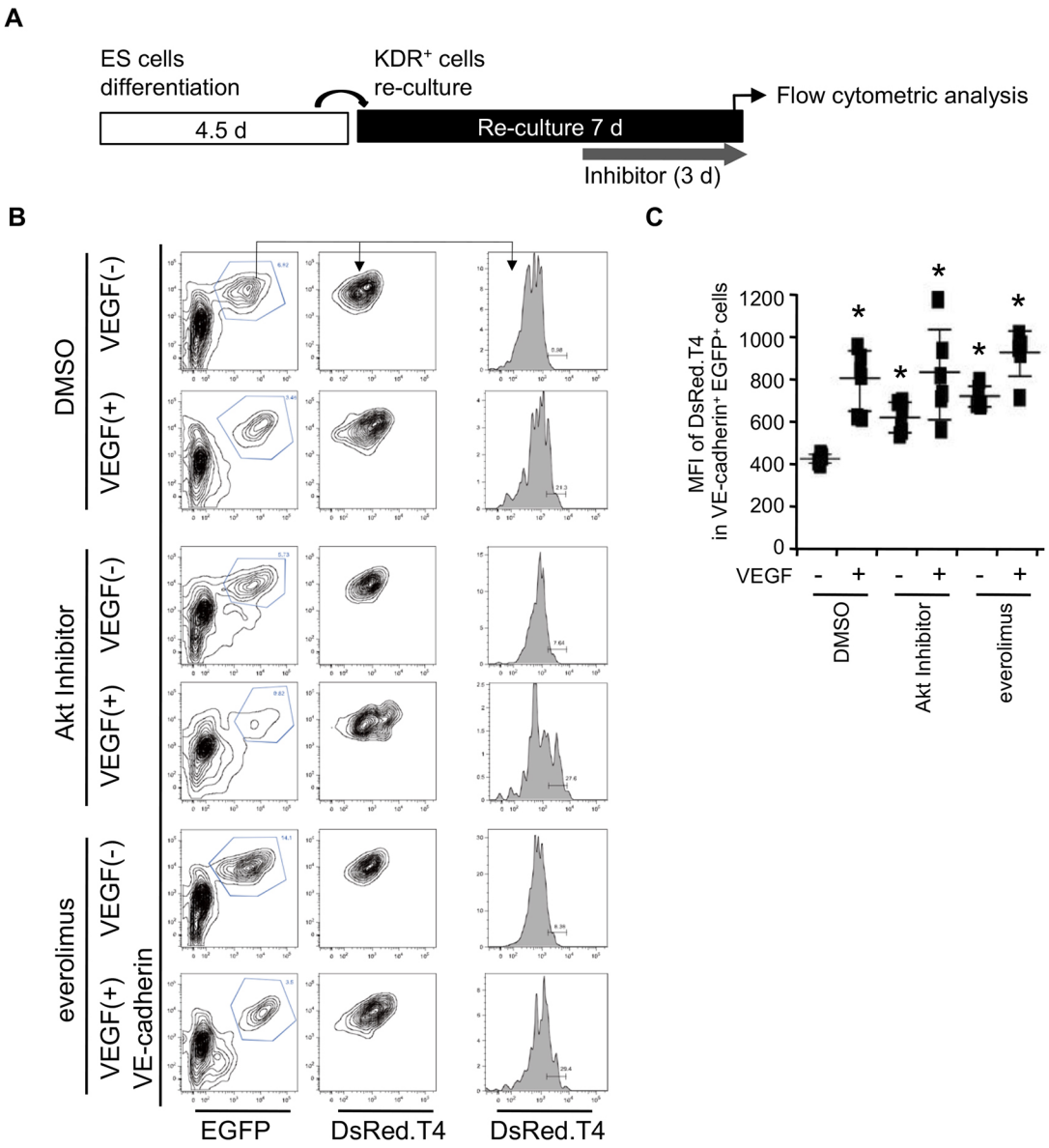

Fig. 5. Activation of the *Tagln* promoter accompanies EC elongation induced by various pathways. KDR$^+$ cells induced from F10-EGFP/Tagln-DsRed.T4 ESCs were cultured on an OP9 cell layer with or without VEGF (10 ng/ml). After 4 days, cells were treated with 5 µM chemical inhibitors (Akt inhibitor VIII or everolimus) or DMSO as a vehicle control, and were incubated for a further 3 days. Expression of EGFP, VE-cadherin and DsRed.T4 were analyzed using flow cytometry. (A) Experimental design for ESC differentiation and inhibitor treatment. (B) Flow cytometric analysis of DsRed.T4 expression in ECs. VE-cadherin$^+$ EGFP$^+$ ECs were gated (left column; gated population is outlined and percentage of cells shown), and DsRed.T4 expression of the EC population is shown as contour plots (middle columns) or histograms (right columns; brackets indicate DsRed.T4-positive population and percentage of cells shown). (C) Mean fluorescence intensity (MFI) of DsRed.T4 in the EC populations was calculated from the histograms shown in B. Results are presented as the mean±s.d. (n=6 per group). Data were analyzed using Dunnett's test [*P<0.05 compared with the DMSO-treated VEGF(-) control]. Similar results were obtained from two independent experiments using two clones.

been demonstrated by co-immunoprecipitation in human colorectal cancer cell lines (Lew et al., 2020; Zhong et al., 2020; Zhou et al., 2020). Thus, the effects of TAGLN on angiogenesis may also require the appropriate cooperation and involvement of other relevant factors.

It may be seemingly inconsistent that the expression of *Tagln*, which negatively regulates angiogenesis, is activated in angiogenic culture models containing VEGF, a potent angiogenic factor. Transcriptional regulation of the *Tagln* gene in SMCs has been well studied (for reviews see Mack, 2011; Owens et al., 2004). Transcription of the *Tagln* gene is dependent on binding of serum response factor (SRF) to CArG elements in its promoter (Kim et al., 1997). The expression level of *SRF* has been reported to be increased by VEGF in HUVECs and rat gastric microvascular endothelial cells (RGMECs), and SRF is translocated into the nucleus in RGMECs stimulated with VEGF (Chai et al., 2004). These reports may partially explain the activation of *Tagln* expression in ECs in the presence of VEGF.

SRF forms a complex with NK3 homeo box 2 (NKX3-2) and GATA-binding protein 6 (GATA6), and cooperatively transactivates the *Tagln* promoter (Nishida et al., 2002). Myocardin, another cofactor of SRF, also provides SMC specificity to the *Tagln* promoter transactivation (Du et al., 2003). SMAD family member 3 (SMAD3) and Kruppel-like factor 5 (KLF5) transactivate the *Tagln* promoter in fibroblasts stimulated with TGF-β (Adam et al., 2000;

Journal of Cell Science (2021) 134, jcs254920. doi:10.1242/jcs.254920

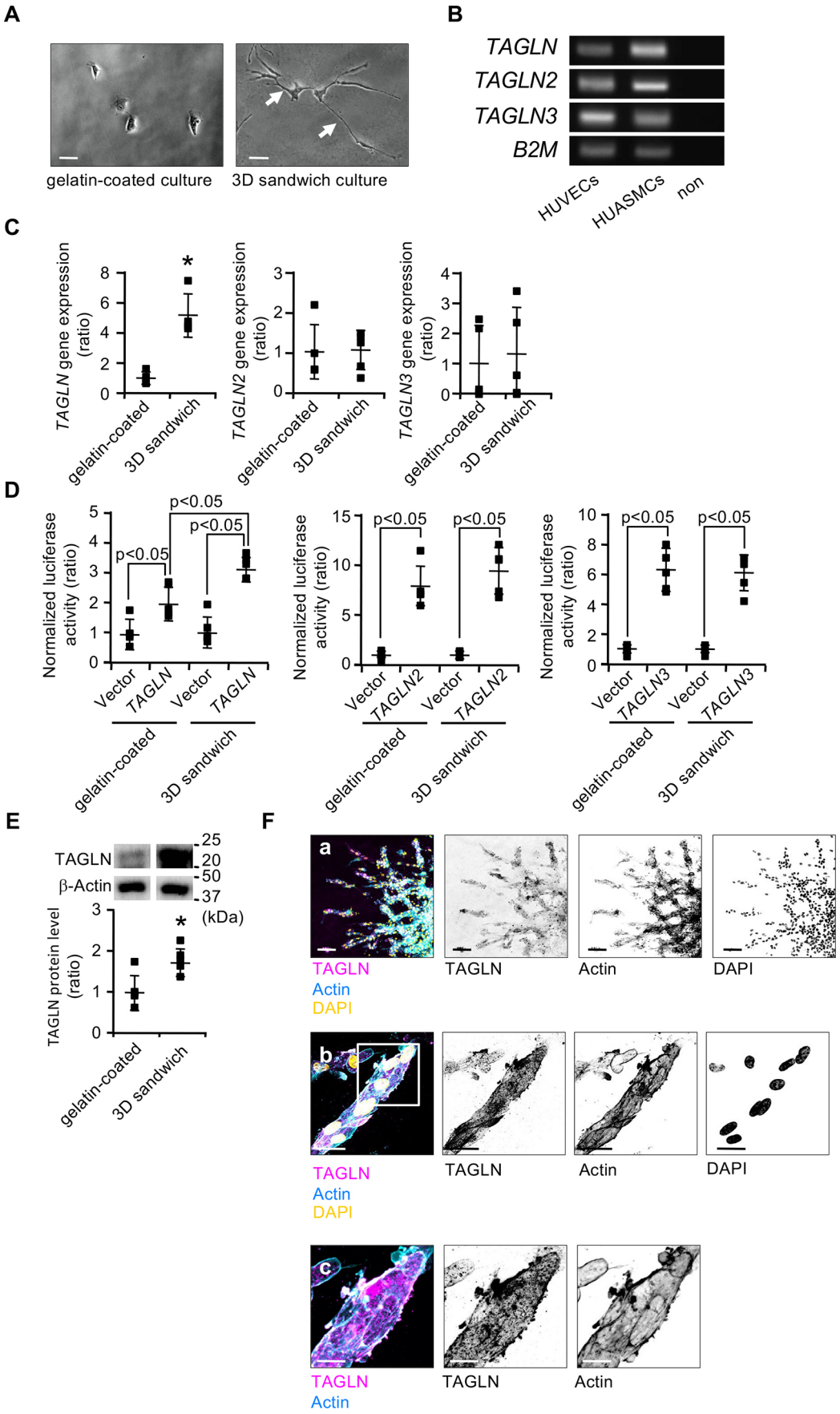

Fig. 6. See next page for legend.

Fig. 6. *TAGLN* expression and promoter activity are increased in elongated primary ECs. (A–E) HUVECs were cultured on a gelatin-coated plate (gelatin-coated culture) or between two layers of type I collagen gel (3D sandwich culture) in the presence of VEGF (10 ng/ml). (A) Phase-contrast images after 1 day of culture. White arrows indicate elongated cells. Scale bars: 40 µm. Similar results were obtained in three independent experiments. (B) The mRNA expression of *TAGLN* isoforms in HUVECs in gelatin-coated culture and HUASMCs was detected using RT-PCR. β-2 microglobulin (*B2M*) and non (H_2O) show an internal control and a no-template negative control, respectively. Similar results were obtained in three independent experiments. (C) The mRNA expression level of *TAGLN* isoforms was determined using real-time quantitative PCR analysis. Data were normalized to *B2M* and are presented as fold change relative to the control (mean±s.d., *n*=5 from five independent experiments). The data were analyzed using an *F*-test, followed by an unpaired two-tailed *t*-test (**P*<0.05). (D) Luciferase reporter assay of the promoter activity of *TAGLN* isoforms was performed after 2 days of culture. The reporter activity was normalized to *Renilla* luciferase (pRL-SV40) activity for transfection efficiency. Data are presented as a ratio relative to firefly luciferase vector-only control (pGL4.15 vector) in the gelatin-coated culture (mean±s.d., *n*=5 per group). The results were analyzed using Tukey's test. Similar results were obtained in three independent experiments. (E) Western blot analysis using an antibody against the TAGLN protein (ab14106, Abcam). Top: western blot images. β-actin protein was used as an internal control. Bottom: expression levels were normalized to β-actin. Data are presented as a ratio relative to the expression in gelatin-coated culture (mean±s.d., *n*=5 from five independent experiments). The data were analyzed using an *F*-test, followed by an unpaired two-tailed *t*-test (**P*<0.05 compared with the gelatin-coated culture). (F) Aggregates of HUVECs were mounted in type I collagen gel and cultured in the presence of VEGF (10 ng/ml) for 3 days to induce vessel-like structures. Micrographs show TAGLN (ab14106, Abcam; magenta), actin (cyan) and DAPI (yellow) staining. Single-channel images are shown in inverted grayscale. The boxed region in panel b is shown at higher magnification in panel c. Scale bars: 100 µm (a), 20 µm (b), 10 µm (c). Similar results were obtained in three independent experiments.

Qiu et al., 2003). Our previous gene expression analyses of ESC-derived ECs using a DNA microarray indicated significant expression of *Srf*, *Nkx3-2* and *Gata6*, regardless of whether or not ECs had been stimulated with VEGF (NCBI GEO accession GSE76366; Tsuji-Tamura and Ogawa, 2016). In the same study, expression of *myocardin*, *Smad3* and *Klf5* was barely detectable. A set of regulatory molecules that transactivates the *Tagln* promoter in ECs might be different from those present in SMCs, and further studies will be needed to explore the mechanism of *Tagln* gene activation in ECs.

In conclusion, our findings suggest that TAGLN is induced in elongating angiogenic ECs and is involved in the regulation of angiogenesis. Elevated expression of the *TAGLN* isoforms has been documented in pathological ECs in tumors and gestational diabetes mellitus with vascular dysfunction (Jin et al., 2016; Varberg et al., 2018; Wang et al., 2019). Therefore, this new role of TAGLN should contribute to our understanding of molecular mechanisms underlying the regulation of physiological and pathological angiogenesis.

MATERIALS AND METHODS

Cells

All clones of F10-EGFP/Tagln-DsRed.T4 mouse ESCs were constructed by the introduction of two fluorescent reporters into KTPU8 ESCs (Tsuji-Tamura and Ogawa, 2016), which is a feeder-free subline of TT2 ES cells derived from the F1 embryo (C57BL/6×CBA) (Nakahara et al., 2013; Yagi et al., 1993). F10-EGFP/Tagln-DsRed.T4 ESCs and OP9 stromal cells (Kodama et al., 1994) were maintained as previously described (Park et al., 2009). HUVECs (Cellworks, Buckingham, UK) were cultured on gelatin-coated plates in Dulbecco's modified Eagle's medium/F12 (DMEM/F12; Nacalai Tesque, Inc., Kyoto Japan) supplemented with 10% fetal bovine serum (FBS, PAA Laboratories, Linz, Austria) and 10 ng/ml basic fibroblast growth factor (b-FGF; NBP2-35152; Novus Biologicals, CO, USA). HUVECs were passaged by dissociation using 0.05% trypsin (T3924; Sigma-Aldrich, St Louis, MO, USA) and were used until passage seven. A mouse vascular SMC line (MOVAS; ATCC, Manassas, VA, USA) were cultured in DMEM (Thermo Fisher Scientific, Waltham, MA, USA) supplemented with 10% FBS. Human umbilical artery smooth muscle cells (HUASMCs) were obtained from PromoCell (Heidelberg, Germany) for total RNA extraction.

Animals

All experiments conducted using animals were approved by the Animal Care and Use Committee of Kumamoto University and the Committee on Animal Experimentation of Hokkaido University, and were performed according to institutional guidelines that conformed to the Guidelines for Proper Conduct of Animal Experiments (Science Council of Japan, June 1, 2006) and the Law for the Humane Treatment and Management of Animals (Law No. 105, 1973) in Japan. Pregnant ICR mice were obtained from Kyudo Co. Ltd. (Saga, Japan) and Japan SLC (Shizuoka, Japan). All mice were quickly killed by cervical dislocation without anesthesia following guidelines for the euthanasia of animals of the American Veterinary Medical Association (AVMA; https://www.avma.org/), and then the embryos were obtained.

Chemical inhibitors and antibodies

LY294002 (129-04861) and rapamycin (184-01311) were purchased from Wako Pure Chemical Industries (Osaka, Japan). Akt inhibitor VIII, isozyme selective (124018), was purchased from Calbiochem (La Jolla, CA, USA). Everolimus (S1120) was purchased from Selleck Chemicals (Houston, TX, USA). Rabbit polyclonal anti-TAGLN antibody (1:1000; ab14106, Abcam), rabbit polyclonal IgG isotype control (1:1000; ab27472), rabbit polyclonal anti-green fluorescent protein (GFP) antibody (1:1000; ab6556), CytoPainter Phalloidin-iFluor 488 Reagent (ab176753) and CytoPainter Phalloidin-iFluor 555 Reagent (ab176756) were purchased from Abcam (Cambridge, MA, USA). FITC-conjugated isolectin B4 (L2895), mouse monoclonal anti-α smooth muscle actin (αSMA) antibody (1:1000; A2547) and rabbit polyclonal anti-TAGLN antibody (1:1000; HPA019467) were purchased from Sigma-Aldrich. Mouse monoclonal anti-desmin antibody (1:1000; M0760) was purchased from Dako Cytomation (Glostrup, Denmark). Mouse monoclonal anti-GFP antibody (1:1000; 012-20461) was purchased from Wako. Rabbit polyclonal anti-red fluorescent protein (RFP) (1:1000; 600-401-379) was purchased from Rockland Immunochemicals Inc. (Limerick, PA, USA). Rat monoclonal anti-KDR antibody (Avas12; Kataoka et al., 1997) and rat monoclonal anti-VE-cadherin antibody (2B12; Matsuyoshi et al., 1997) were purified from culture supernatants from hybridomas using CELLine (353137, BD Biosciences, San Jose, CA, USA). The allophycocyanin (APC)-conjugated anti-KDR antibody was prepared from Avas12 using APC Labeling Kit-NH2 (LK21, Dojindo, Kumamoto, Japan). Rabbit polyclonal anti-beta actin antibody (1:1000; 20536-1-AP) was purchased from Proteintech (Chicago, IL, USA). Alexa Fluor 488-conjugated goat anti-rabbit IgG (ab150077, Abcam), Alexa Fluor 555-conjugated goat anti-rabbit IgG (A-21429, Molecular Probes), Alexa Fluor 488-conjugated goat anti-mouse IgG (ab150113, Abcam), Alexa Fluor 546-conjugated goat anti-mouse IgG (A-11030, Molecular Probes), Alexa Fluor 647-conjugated goat anti-mouse IgG (A-21236, Molecular Probes), Alexa Fluor 555-conjugated goat anti-rat IgG (A-21434, Thermo Fisher Scientific, Waltham, MA, USA) and Alexa Fluor 647-conjugated goat anti-rat IgG (A-21247, Molecular Probes) were used as secondary antibodies.

ESC differentiation, FACS analysis and cell sorting

ESCs were cultured on an OP9 cell layer for 3.5–4.5 days in α-modified Eagle's medium (α-MEM; Thermo Fisher Scientific) supplemented with 10% fetal calf serum (FCS; Corning, Woodland, CA, USA) and 50 µM 2-mercaptoethanol to induce differentiation into KDR^+ mesodermal cells, as previously described (Park et al., 2009). Cultured cells were non-enzymatically dissociated by incubating with a Cell Dissociation Buffer (Thermo Fisher Scientific). Following suspending in normal mouse serum (Merck, Darmstadt, Germany) to block nonspecific binding, cells were

Journal of Cell Science (2021) 134, jcs254920. doi:10.1242/jcs.254920

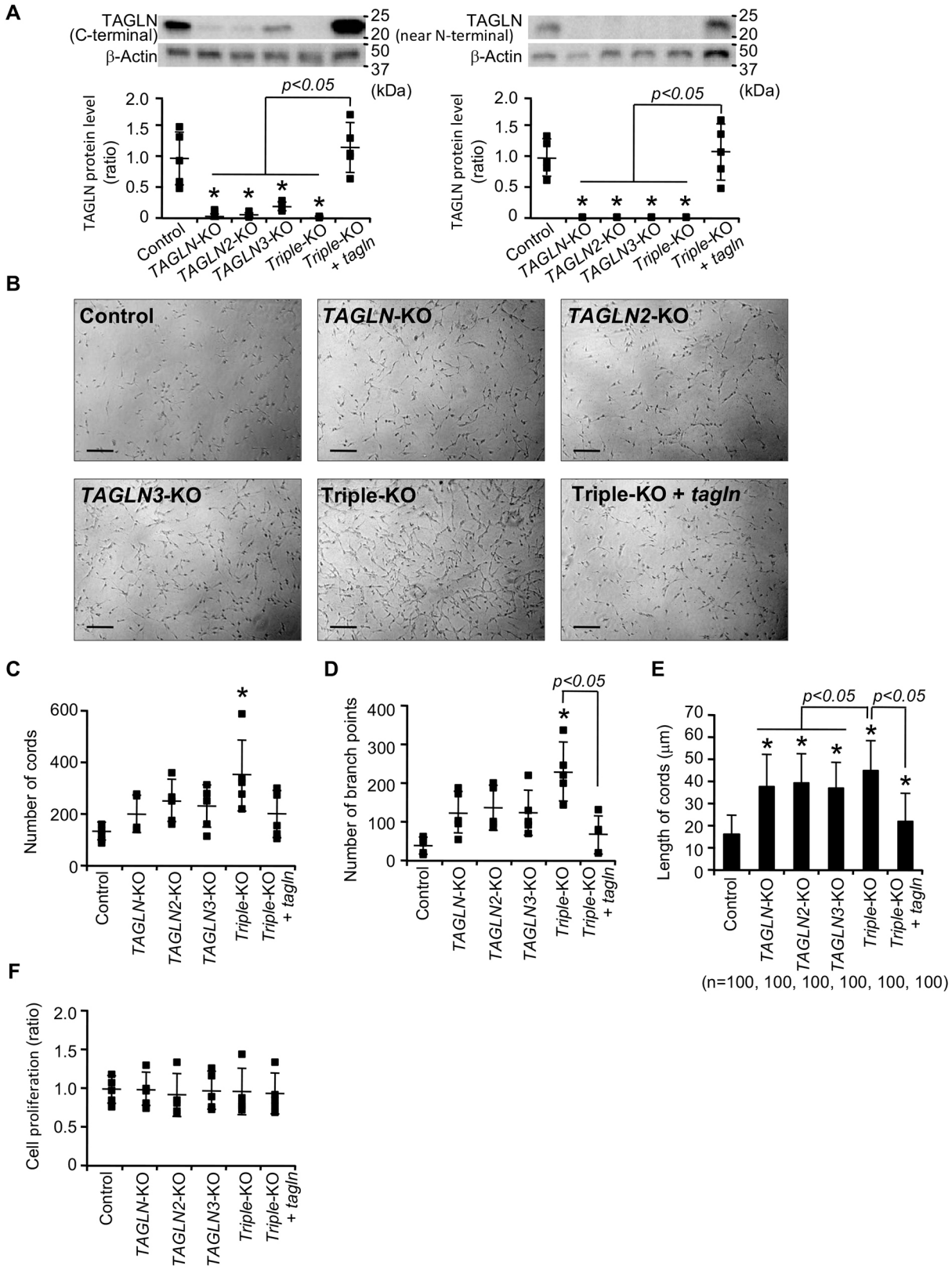

Fig. 7. See next page for legend.

incubated with APC-conjugated anti-KDR antibody for 30 min at 4°C. For differentiation of ECs, KDR^+ cells were purified by fluorescence-activated cell sorting (FACS) using a special order FACSAria II cell sorter (BD Bioscience, San Jose, CA, USA). KDR^+ cells were re-cultured on an OP9 cell layer in the presence or absence of recombinant mouse VEGF-A_{165} (referred to here as VEGF; 10 ng/ml; 450-32; Peprotech, Rocky Hill, NJ, USA) for 4 or 7 days. The mean fluorescence intensity (MFI) of the DsRed.T4 signal was determined using the special order FACSAria II cell sorter and FlowJo software (FlowJo, LLC., Ashland, OR, USA). For differentiation of SMCs, purified KDR^+ cells were cultured on an OP9 cell

Journal of Cell Science

Journal of Cell Science (2021) 134, jcs254920. doi:10.1242/jcs.254920

Fig. 7. Single and triple-knockout of *TAGLN*, *TAGLN2* and *TAGLN3* causes excessive cord-like structure formation. HUVECs were genetically edited in the *TAGLN*, *TAGLN2* and *TAGLN3* genes using the CRISPR/Cas9 system, and rescue of expression was conducted using zebrafish *tagln*, creating single knockout cell lines (*TAGLN*-KO, *TAGLN2*-KO and *TAGLN3*-KO), a *TAGLN* isoform triple knockout (triple-KO) and the *tagln*-expression-rescued triple-KO (triple-KO+*tagln*). (A) Western blot analysis using antibodies against either the C-terminal region (ab14106, Abcam; left panel) or the near N-terminal region (HPA019467, Sigma-Aldrich; right panel) of the TAGLN protein. Top: western blot images. β-actin protein was used as an internal control. Similar results were obtained in five independent experiments. Bottom: expression levels were normalized to β-actin. Data are presented as a ratio relative to the control group (mean±s.d., n=5). The data were analyzed using Tukey's test (*P<0.05 compared with the control group). (B–E) Genetically edited and transfected HUVECs were grown in 3D sandwich culture in the presence of VEGF (10 ng/ml) for 1 day. (B) Phase-contrast images. Scale bars: 200 µm. Similar results were obtained in three independent experiments. (C,D) The number of cord-like structures (C) and branch points (D) per field is presented as the mean±s.d. (n=5 fields per group). The data were analyzed using Tukey's test (*P<0.05). (E) The length of the cord-like structures is presented as the mean±s.d. The total number of cords examined is indicated in brackets. The data were analyzed using Tukey's test (*P<0.05 compared with the control). (F) Cell proliferation assay. Results are presented as the mean±s.d. (n=5 per group). The data were analyzed using Dunnett's test (comparison to the control). No significant difference was found. Similar results were obtained in three independent experiments.

layer for 7 days. KDR$^-$ EGFP$^-$ DsRed.T4$^+$ cells were purified by FACS and re-cultured on a gelatin-coated culture plate for 2 days.

Immunofluorescence microscopy

Immunofluorescence staining was performed as previously described (Matsukawa et al., 2009; Park et al., 2009). Whole-mount immunostaining of embryonic day (E) 11.5 embryos was performed as described by Yokomizo and Dzierzak (2010). Fluorescence images were taken using an FV1000D confocal laser-scanning microscope and imaging software (Olympus, Tokyo, Japan). When necessary, contrast and brightness were adjusted uniformly over original images to observe cell morphology clearly. The gamma setting was not changed. ECs were manually classified according to cell shape. The fluorescence intensity of images was determined using the plot profile tool of ImageJ (National Institutes of Health, Bethesda, MD).

Live-cell imaging

EGFP and DsRed.T4 images of living cells were taken using an IN Cell Analyzer 6000 laser line-scanning confocal imaging system (GE Healthcare Life Sciences, Buckinghamshire, UK). Original images were uniformly processed to adjust the contrast and brightness, and were subjected to grayscale inversion using ImageJ software to allow detailed observation of cell morphological changes. EC colonies were manually classified according to morphology.

3D spheroid culture for the formation of vessel-like structures

Induction of an ESC-derived vessel-like structure in 3D spheroid culture was performed as previously described (Park et al., 2009; Yamashita et al., 2000). In brief, ESC-derived KDR$^+$ cells were aggregated by incubating in 96-well round-bottomed Sumilon cell-tight spheroid plates (Sumitomo Bakelite Co., Ltd., Tokyo, Japan) in α-MEM containing 10% FCS and VEGF (10 ng/ml). After 1 day, cell aggregates were settled in type I collagen gel (1.5 mg/ml; Nitta Gelatin, Osaka, Japan) containing α-MEM, 10% FCS and VEGF (10 ng/ml), followed by incubation for 4 days. The 3D spheroid culture of HUVECs was the same as described above, except that cells were cultured in DMEM/F12 medium containing 10% FBS and VEGF (10 ng/ml) for 3 days.

Isolation of ECs from KTPU8 and EB5

Mouse ESCs, KTPU8 and EB5 (a subline derived from E14tg2a ES cells) were maintained as previously described (Guo et al., 2007; Nakahara et al., 2013). For induction of ECs, ESCs were cultured on the OP9 cell layer for 4 days in differentiation medium as described above. KDR$^+$ cells were isolated using FACs with phycoerythrin (PE)-conjugated anti-KDR (Avas12; 1:50; BioLegend) monoclonal antibody and re-cultured with OP9 cells for 4 days in differentiation medium with or without 10 ng/ml VEGF. CD45$^-$ VE-cadherin$^+$ CD31$^+$ KDR$^+$ ECs were sorted using following monoclonal antibodies; CD45–APC (30-F11; 1:100; BioLegend), VE-cadherin–Brilliant Violet (BV) 421 (BV13; 1:167; BioLegend), CD31–fluorescein isothiocyanate (FITC) (390; 1:100; BioLegend), and KDR–PE (Avas12; 1:50; BioLegend).

Real-time quantitative PCR analysis and detection of gene expression

Total RNA was extracted using QIAzol lysis reagent (79306, Qiagen), and reverse transcribed using PrimeScript RT Master Mix (RR036A; Takara Bio Inc., Shiga, Japan). The QuantiTect SYBR Green PCR kit (Qiagen) was used for quantitative real-time PCR reactions with a StepOne Real-Time PCR System (ABI, Foster City, CA, USA). To detect gene expression, target transcripts were amplified using a Taq PCR Core Kit (201223, Qiagen) and a standard thermal cycler (ASTEC PC707, Japan). Amplified products were separated on 1.5% agarose gels followed by staining with SYBR Gold Nucleic Acid Gel Stain (S11494, Thermo Fisher Scientific). Gel images were obtained using a UV transilluminator (Red Imaging System; Alpha Innotech, San Diego, CA, USA). The primers used for PCR are described below.

Primers for real-time quantitative PCR

The following primers were used: mouse *Tagln*, forward (fwd) 5′-ATCCCAACTGGTTTATGAAGAAAGC-3′ and reverse (rev) 5′-AAGGCCAATGACGTGCTTCC-3′; mouse *Tagln2*, fwd 5′-GCAGCGGACACTAATGAACC-3′ and rev 5′-AACCCAATCACGTTCTTGCC-3′; mouse *Tagln3*, fwd 5′-GAGGACTCTGATGGCCTTGG-3′ and rev 5′-ATCCTCTCCGATTCTGCTGG-3′; mouse *B2m*, fwd 5′-CTGACCGGCCTGTATGCTAT-3′ and rev 5′-CCGTTCTTCAGCATTTGGAT-3′; human *TAGLN*, fwd 5′-GCAAAGACATGGCAGCAGT-3′ and rev 5′-GCTGGCTCTCTGTGAATTCC-3′; human *TAGLN2*, fwd 5′-CCGAGATGATGGGCTCTTC-3′ and rev 5′-TGGTGCCCATCTGTAACCC-3′; human *TAGLN3*, fwd 5′-CGACATCTTTCAGACGGTGG-3′ and rev 5′-GAAGCTGCTCCTCGGAAAAG-3′; and human *B2M*, fwd 5′-ACTCTCTCTTTCTGGCCTGG-3′ and rev 5′-CTCCTCGGAAAAGCCTCTCC-3′.

Primers for detection of gene expression

The following primers were used: mouse *Tagln*, fwd 5′-ATCCCAACTGGTTTATGAAGAAAGC-3′ and rev 5′-AAGGCCAATGACGTGCTTCC-3′; mouse *Tagln2*, fwd 5′-CTTCCAGAAGTGGCTCAAGG-3′ and rev 5′-ATCACGTTCTTGCCCTCTTG-3′; mouse *Tagln3*, fwd 5′-CCTGCAGTGTGCTGAGGATA-3′ and rev 5′-TAACTGCAACACTGCCCAAG-3′; mouse *Cdh5*, fwd 5′-AAGTTTGCCCTGAAGAACGA-3′ and rev 5′-ACCCCGTTGTCTGAGATGAG-3′; mouse *Acta2*, fwd 5′-CCGAGATCTCACCGACTACC-3′ and rev 5′-TCAGGCAGTTCGTAGCTCTT-3′; mouse *B2m*, fwd 5′-CTGACCGGCCTGTATGCTAT-3′ and rev 5′-CCGTTCTTCAGCATTTGGAT-3′; human *TAGLN*, fwd 5′-GCAAAGACATGGCAGCAGT-3′ and rev 5′-GCTGGCTCTCTGTGAATTCC-3′; human *TAGLN2*, fwd 5′-CCGAGATGATGGGCTCTTC-3′ and rev 5′-TGGTGCCCATCTGTAACCC-3′; human *TAGLN3*, fwd 5′-GTTGCAGTCACCAAGGATGA-3′ and rev 5′-GAAGCTGCTCCTCGGAAAAG-3′; human *B2M*, fwd 5′-ACTCTCTCTTTCTGGCCTGG-3′ and rev 5′-ATGTCGGATGGATGAAACCC-3′.

3D sandwich culture for the formation of cord structures

Type I collagen gel (1.5 mg/ml) was plated as a bottom layer in 24-well plates and allowed to polymerize at 37°C for 10 min. HUVECs were precultured on the bottom layer (2×10^4 or 1×10^4 cells per well, depending on the experiment) in DMEM/F12 containing 10% FBS. After 4 h, the medium was gently aspirated, and type I collagen gel as a top layer was added on cultured cells. After 10 min of incubation at 37°C for gel polymerization, the cells were cultured in DMEM/F12 containing 10% FBS

Journal of Cell Science (2021) 134, jcs254920. doi:10.1242/jcs.254920

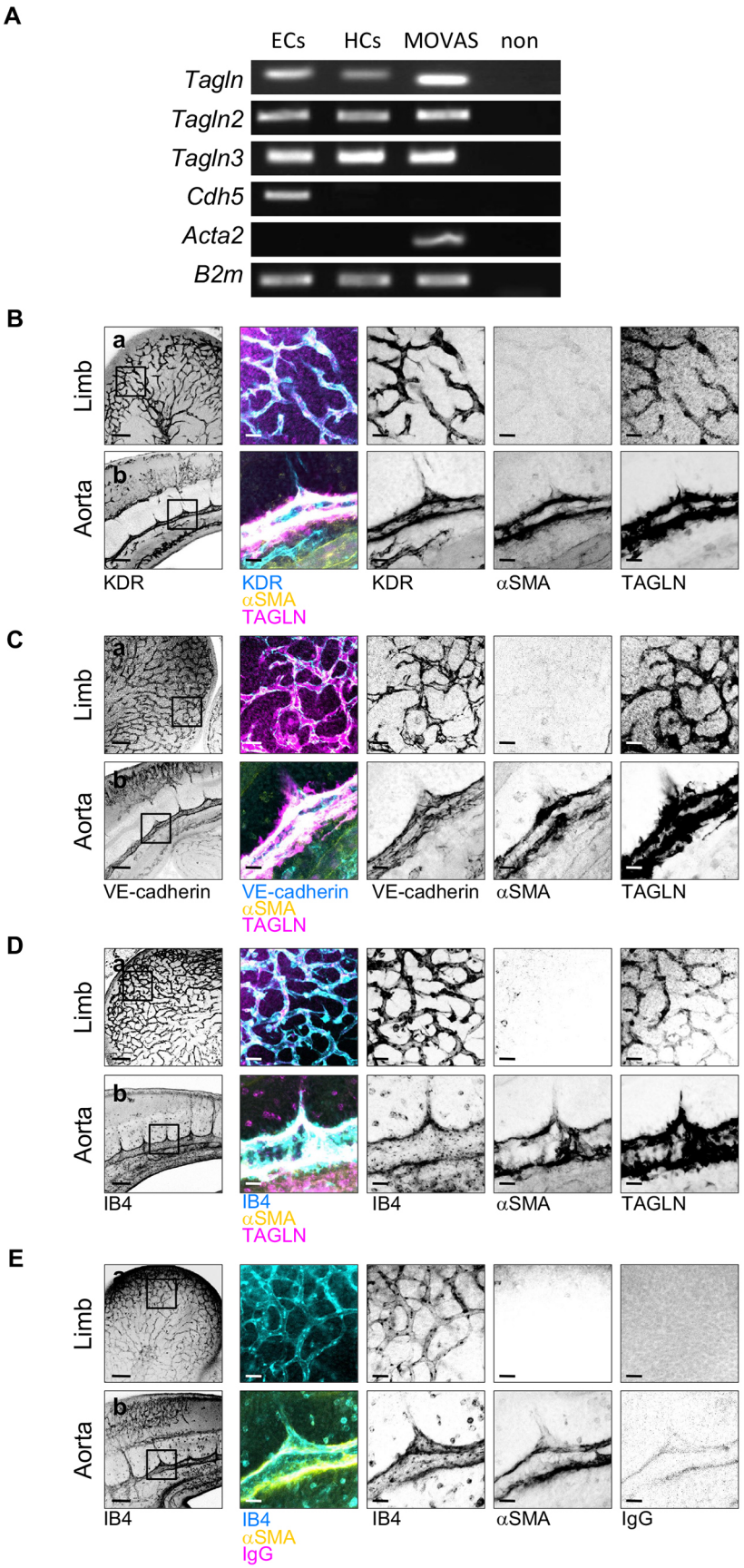

Fig. 8. ECs in the developing mouse embryo express *Tagln* isoforms. (A) VE-cadherin$^+$ KDR$^+$ CD31$^+$ CD45$^-$ ECs and CD45$^+$ hematopoietic cells (HCs) were sorted from E10.5 mouse embryos. The mRNA expression of *Tagln* isoforms, *Cdh5* (which encodes VE-cadherin) and *Acta2* (which encodes αSMA) was detected using RT-PCR. The MOVAS cell line was used as an SMC population. *B2m* and non (H_2O) show an internal control and a no-template negative control, respectively. Similar results were obtained from three independent experiments using different litters of embryos. (B–E) Limb vessels and dorsal aortae were investigated by whole-mount immunostaining of E11.5 mouse embryos. (B) Immunostaining of KDR (cyan), αSMA (yellow) and TAGLN (ab14106, Abcam; magenta). (C) Immunostaining of VE-cadherin (cyan), αSMA (yellow) and TAGLN (ab14106, Abcam; magenta). (D) Immunostaining of isolectin B4 (IB4; cyan), αSMA (yellow) and TAGLN (ab14106, Abcam; magenta). (E) Immunostaining of IB4 (cyan), αSMA (yellow) and IgG isotype-matched control (magenta). Right-hand panels show higher magnification of the boxed area in each left-most panel (a, limb; b, aorta). Single-channel images are shown in inverted grayscale. Scale bars: 100 µm (left panels), 20 µm (right panels). Similar results were obtained from embryos of six different litters.

Journal of Cell Science (2021) 134, jcs254920. doi:10.1242/jcs.254920

and VEGF (10 ng/ml) for 1 day. Images of vascular cords were captured using an ECLIPSE TS100 inverted microscope equipped with a DS-Fi3 Digital Camera (Nikon Corporation, Tokyo, Japan). Images were converted to 8-bit RGB color using ImageJ. Brightness and contrast adjustment was uniformly applied to the entire image for the detailed observation of vascular cord structures. The number of vascular cords per field was manually determined. Cross-points of the vascular cords were counted as branch points. The length of the vascular cords was determined by manual tracing.

Luciferase reporter assay

The *TAGLN* promoter (GenBank accession NC_000011.10, bases 117198943–117199470; Camoretti-Mercado et al., 1998) and the upstream sequence of *TAGLN2* (GenBank accession NC_000001.11, bases 159925141–159926847) and *TAGLN3* (GenBank accession NC_000003.12, bases 111997537–111999395) were amplified from human genomic DNA by PCR using the following primers (In-Fusion cloning sites are underlined): promoter of *TAGLN*, fwd 5′-GCTCGCTAGCCTCGATGTCCCCACAAACCCCTG-3′ and rev 5′-AGGCCAGATCTTGATAGCCCAACTTCCCTCCAAG-3′; upstream sequence of *TAGLN2*, fwd 5′-GCTCGCTAGCCTCGACACGCCTTTGCCCTTGAG-3′ and rev 5′-AGGCCAGATCTTGATTTTTCCCCTCGCCCCAGT-3′; upstream sequence of *TAGLN3*, fwd 5′-GCTCGCTAGCCTCGAGCAAACCACCCACATATCTCC-3′ and rev 5′-AGGCCAGATCTTGATGCATCCACACAATAGCAGCA-3′. The PCR products were inserted into the multi-cloning site of a pGL4.15 firefly luciferase reporter vector (E6701; Promega, Madison, WI, USA) using the In-Fusion HD Cloning Kit (Z9648N, Takara). The vectors were co-transfected with pRL-SV40 (E2231, Promega) into HUVECs using ScreenFect A plus (293-77101, Wako) and SFA P-reagent (191-18331, Wako). Luciferase activity was revealed using the Dual Luciferase Reporter Assay System (E1910, Promega) and quantified using a Mini Lumat LB 9506 (Berthold Technologies, Bad Wildbad, Germany).

Western blotting

HUVECs were lysed in ice-cold CelLytic M Cell Lysis Reagent (C2978, Sigma-Aldrich) containing cOmplete Mini Protease Inhibitor Cocktail (04693124001, Sigma-Aldrich) for 15 min. Cell lysates were centrifuged at 13,000 ***g*** for 15 min at 4°C, and the supernatants were mixed with Laemmli sample buffer (1610747, Bio-Rad, Hercules, CA, USA). After heating for 5 min at 98°C, proteins were separated on a 10% SDS–PAGE gel and transferred to PVDF membranes using a Trans-Blot SD Semi-Dry transfer cell (Bio-Rad). Membranes were blocked in 2% blocking reagent or skim milk in TBS-T buffer [20 mM Tris-HCl (pH 7.6), 137 mM NaCl and 0.1% Tween 20] overnight at 4°C. Membranes were incubated with primary antibodies in TBS-T buffer overnight at 4°C, rinsed and incubated with horseradish peroxidase-conjugated donkey anti-rabbit IgG antibody (NA934; Amersham, Buckinghamshire, UK) for 2 h at room temperature. Signals were revealed using ECL Prime Western Blotting Detection Reagent (RPN2232, Amersham) and detected using an image analyzer LAS-1000 (Fujifilm, Tokyo, Japan). The target protein bands were quantified by densitometry using ImageJ.

Targeted gene knockout, expression recovery and overexpression

The CRISPR/Cas9-mediated genome editing system was used for targeted knockout of *TAGLN*, *TAGLN2* and *TAGLN3* genes in HUVECs. Guide sequences were designed by the CRISPR gRNA design tools of ATUM (https://www.atum.bio/eCommerce/cas9/input) and CRISPR direct (https://crispr.dbcls.jp). Synthesized guide sequences were cloned into pX459.V2.0 (plasmid #62988, Addgene), which expresses gRNA, Cas9 nuclease and a puromycin-resistance gene, using the Golden Gate cloning protocol (https://media.addgene.org/cms/filer_public/3e/e1/3ee1ce9c-99f9-4074-9a28-109d34971471/zhang-lab-sam-cloning-protocol.pdf). The following target and PAM sequences were used (PAM sequences are underlined): *TAGLN*, 5′-CGCCCAGACCGTGGGCGCTTGGG-3′; *TAGLN2*, 5′-GGGGCCGGCCCACATCCTTTCGG-3′; and *TAGLN3*, 5′-GATCATCCTGCAGTGCGCCGAGG-3′. Plasmids expressing zebrafish or mouse TAGLN were used for recovery or overexpression studies. The cDNA sequences encoding full-length zebrafish *tagln* (NM_001045467.1) or mouse *Tagln* (NM_011526.5) were amplified by PCR using the following primers (In-Fusion cloning sites are underlined and Kozak sequences are in lowercase): zebrafish *tagln*, fwd 5′-CAAAGAATTCCTCGAgccaccATGGCAAACAAGGGGCCGTC-3′ and rev 5′-TCGAGCGGCCGCGGGCGTCAGTGTTTTGAAT-3′; mouse *Tagln*, fwd 5′-CAAAGAATTCCTCGAgccaccATGGCCAACAAG-3′ and rev 5′-GCTTATCGAGCGGCCGGGCTGGCCTTCCCTTTC-3′. Zebrafish *tagln* or mouse *Tagln* cDNA was inserted into the multiple cloning site of the pCAG-Ipuro vector (Niwa et al., 1991), which contains the CAG promoter, an internal ribosome entry site and a puromycin-resistance gene, using an In-Fusion HD Cloning Kit (Z9648N, Takara). The vectors were transfected into HUVECs using ScreenFect A plus and SFA P-reagent (293-77101 and 191-18331, respectively; Wako). After 1 day, puromycin selection at 5 µg/ml was initiated and maintained for 3 days to eliminate non-transduced cells. The results of genome editing were confirmed by genomic sequencing.

Analysis of migration by *in vitro* scratch-wound assay

HUVECs were genetically edited in the *TAGLN*, *TAGLN2* and *TAGLN3* genes using the CRISPR/Cas9 system, and transfected to rescue expression using zebrafish *tagln* to create the following cell lines: *TAGLN*, *TAGLN2*, and *TAGLN3* single knockouts (KO); *TAGLN* isoform triple knockout (triple-KO); and *tagln*-expression-rescued triple-KO (triple-KO+*tagln*). Cells were seeded at the same density on gelatin-coated plates. When the cells become nearly confluent, the cell monolayers were scratched and wounded using a universal cell scraper. After washing with phosphate-buffered saline (PBS), cells were incubated in DMEM/F12 containing 10% FBS at 37°C for 4 h. Images of scratched areas were acquired using an ECLIPSE TS100 inverted microscope (Nikon Corporation) and converted to 8-bit RGB color using ImageJ. Brightness and contrast adjustments were uniformly applied to the entire image for the detailed observation of scratched areas. For each image, the cell-free areas formed by scratch application were measured by manual tracing using ImageJ. Migration rates were obtained as the percentage area of each scratch closure, which was analyzed by comparing the images from immediately after scratch application (0 h) with images of the end timepoint (4 h).

Cell proliferation assay

HUVECs were seeded at 4×10^3 cells per well in a gelatin-coated 96-well plate and incubated in DMEM/F12 containing 10% FBS and VEGF (10 ng/ml). After 1 day, cells were incubated in a culture medium containing TetraColor ONE (Seikagaku Corp., Tokyo, Japan) for 3 h. Optical density at 450 nm was measured using an iMark microplate reader (Bio-Rad, Hercules, CA, USA).

Targeted gene knockdown by small interfering RNAs

Small interfering RNAs (siRNAs) were used for targeted knockdown of *TAGLN*, *TAGLN2* and *TAGLN3* genes in HUVECs. Silencer Select Pre-Designed siRNA (s13741; Thermo Fisher Scientific, Inc., Waltham, MA, USA) was used for knockdown of *TAGLN*. The following target-specific siRNAs were designed using the siRNA online design site siDirect version 2.0 (http://sidirect2.rnai.jp/): *TAGLN2*, 5′-CAGAAGATTGAGAAACAATATGA-3′; *TAGLN3*, 5′-GTCAAAGATGGCTTTTAAGCAGA-3′. These siRNAs were synthesized by Hokkaido System Science Co., Ltd. (Hokkaido, Japan). HUVECs were transfected with target-specific siRNAs or Silencer Select Negative Control No. 1 siRNA (4390843; Thermo Fisher Scientific, Inc) using Lipofectamine RNAiMAX (13778-100; Invitrogen, Carlsbad, CA, USA).

Cells were used for each experiment 1 or 2 days after transfection. The expression levels of mRNAs and proteins were confirmed using real-time PCR or western blot analysis, respectively.

Isolation of ECs and hematopoietic cells from mouse embryos

E10.5 whole mouse embryos were incubated in 1 mg/ml collagenase/dispase (10269638001; Roche Diagnostics, Mannheim, Germany) at 37°C for 40 min. Tissues were dissociated by gentle pipetting to obtain a single-

cell suspension. Cells were stained with the following monoclonal antibodies: Brilliant Violet 421 anti-mouse VE-cadherin (BV13; 1:167), FITC anti-mouse CD31 (390; 1:100), PE anti-mouse KDR (Avas12; 1:50) and APC anti-mouse CD45 (30-F11; 1:100). These antibodies were obtained from BioLegend (San Diego, CA, USA). $CD45^-$ $CD31^+$ VE-cadherin$^+$ KDR^+ ECs and $CD45^+$ hematopoietic cells (HCs) were sorted using an SH-800 cell sorter (Sony Corp., Tokyo, Japan).

scRNA-seq data analysis

A public scRNA-seq dataset of mouse embryos (Baron et al., 2018) was analyzed to identify *Tagln*-expressing ECs. The dataset was downloaded as an R data object and was loaded into the Seurat package (v.3.1.1) (Butler et al., 2018; Stuart et al., 2019). The highly variable features were identified from the normalized dataset for downstream analysis. PCA was performed on the scaled data, and cells were clustered. To visualize this data, Uniform Manifold Approximation and Projection (UMAP), that is a dimension reduction technique, was run using 546 cells. The EC cluster was extracted (198 cells) and separated into *Tagln*-positive (19 cells) and *Tagln*-negative (179 cells) cells. We identified *Tagln*-positive EC-characterized genes (95 genes) based on $\log_2$ fold change ($\geq$0.322) of the average expression between the two groups. Functional characterization of those *Tagln*-positive EC-specific genes was performed using gene ontology (GO) term enrichment analysis (Ashburner et al., 2000; The Gene Ontology Consortium, 2019). The Panther software (http://pantherdb.org/) was used to calculate enrichment (FDR P<0.05, Fisher's exact test).

For our scRNA-seq dataset, the AGM region and the FL segment were extracted from an E10.5 (35 somite pair) C57BL/6N mouse embryo. Tissues were dissociated using 1 mg/ml collagenase/dispase (Roche Diagnostics) for 5 min at 37°C and 0.25% trypsin-EDTA (Thermo Gibco) for 7 min at 37°C. Cells were washed with 1% BSA in HBSS (14185052; Gibco, Thermo Fisher Scientific) and with 1% BSA in PBS. These cells were resuspended in 0.04% BSA in PBS and evaluated for their cell number and viability (>90%) using a Countess automated cell counter (Thermo). A total of 7000 cells were applied to Chromium Controller (10X Genomics). A Chromium Single Cell 3′ v3.1 kit (10X Genomics) was used to generate oligo(dT)-primed cDNA libraries, which were then sequenced by an Illumina HiSeqX. The raw sequence data were processed using the cellranger count command of Cell Ranger (v5.0.0; 10X genomics). All subsequent analyses were performed in the R environment [v4.0.4 (x64)]. The Seurat package (v4.0.1) was used for analyses including quality control, data normalization, data scaling and visualization. For quality control, cells that expressed <600 genes, <1000 unique molecular identifier (UMI) counts, <0.76 $\log_{10}$(genes detected)/$\log_{10}$(UMI counts), or mitochondrial genes accounting for more than 35% of total genes detected per cell were filtered out. The final dataset contained 7270 cells. To visualize this data, UMAP plots were generated. The arterial EC cluster was extracted (183 cells) and separated into *Tagln*-positive (50 cells) and *Tagln*-negative (133 cells) cells. We identified *Tagln*-positive EC-characterized genes (38 genes) based on $\log_2$ fold-change ($\geq$0.322) of the average expression between the two groups. Functional characterization of those *Tagln*-positive arterial EC-specific genes was performed using GO term enrichment analysis. The Panther software was used to calculate enrichment (FDR P<0.05, Fisher's exact test).

Statistical analysis

For multiple comparisons to control groups, Dunnett's or Tukey's multiple comparison test was performed using the MEPHAS webtool (http://www.gen-info.osaka-u.ac.jp/testdocs/tomocom/dunnett-e.html or http://www.gen-info.osaka-u.ac.jp/testdocs/tomocom/tukey-e.html, respectively). For comparison of two samples, F-test followed by an unpaired, two-tailed t-test was performed. A P-value of <0.05 was considered statistically significant.

Acknowledgements

We thank K. Miike (Department of Kidney Development, IMEG, Kumamoto University) for help with single-cell RNA-seq data analysis. Our greatest thanks go to M. Tamura and M. Sato (Graduate School of Dental Medicine, Hokkaido University) for critical discussion and support of analysis.

Competing interests

The authors declare no competing or financial interests.

Author contributions

Conceptualization: K.T.-T.; Methodology: K.T.-T.; Validation: K.T.-T.; Formal analysis: K.T.-T., S.M.-K.; Investigation: K.T.-T., S.M.-K.; Resources: K.T.-T., S.S., M.O.; Writing - original draft: K.T.-T., M.O.; Writing - review & editing: K.T.-T., S.M.-K., S.S., M.O.; Visualization: K.T.-T.; Supervision: M.O.; Project administration: K.T.-T., M.O.; Funding acquisition: K.T.-T.

Funding

This work was supported by the Japan Society for the Promotion of Science (JSPS; grant numbers KAKENHI 15K1125905 and 18K0978208). This work was partly supported by the program of the Joint Usage/Research Center for Developmental Medicine and the Inter-University Research Network for Trans-Omics Medicine, Institute of Molecular Embryology and Genetics, Kumamoto University.

Data availability

The scRNA-seq data has been deposited in the NCBI GEO database under accession GSE167932.

Peer review history

The peer review history is available online at https://journals.biologists.com/jcs/article-lookup/doi/10.1242/jcs.254920

References

Adam, P. J., Regan, C. P., Hautmann, M. B. and Owens, G. K. (2000). Positive- and negative-acting Krüppel-like transcription factors bind a transforming growth factor β control element required for expression of the smooth muscle cell differentiation marker SM22α in vivo. *J. Biol. Chem.* **275**, 37798-37806. doi:10.1074/jbc.M006323200

Amano, M., Ito, M., Kimura, K., Fukata, Y., Chihara, K., Nakano, T., Matsuura, Y. and Kaibuchi, K. (1996). Phosphorylation and activation of myosin by Rho-associated kinase (Rho-kinase). *J. Biol. Chem.* **271**, 20246-20249. doi:10.1074/jbc.271.34.20246

Aranguren, X. L., Agirre, X., Beerens, M., Coppiello, G., Uriz, M., Vandersmissen, I., Benkheil, M., Panadero, J., Aguado, N., Pascual-Montano, A. et al. (2013). Unraveling a novel transcription factor code determining the human arterial-specific endothelial cell signature. *Blood* **122**, 3982-3992. doi:10.1182/blood-2013-02-483255

Arciniegas, E., Frid, M. G., Douglas, I. S. and Stenmark, K. R. (2007). Perspectives on endothelial-to-mesenchymal transition: potential contribution to vascular remodeling in chronic pulmonary hypertension. *Am. J. Physiol. Lung Cell. Mol. Physiol.* **293**, L1-L8. doi:10.1152/ajplung.00378.2006

Ashburner, M., Ball, C. A., Blake, J. A., Botstein, D., Butler, H., Cherry, J. M., Davis, A. P., Dolinski, K., Dwight, S. S., Eppig, J. T. et al. (2000). Gene ontology: tool for the unification of biology. The Gene Ontology Consortium. *Nat. Genet.* **25**, 25-29. doi:10.1038/75556

Assinder, S. J., Stanton, J.-A. L. and Prasad, P. D. (2009). Transgelin: an actin-binding protein and tumour suppressor. *Int. J. Biochem. Cell Biol.* **41**, 482-486. doi:10.1016/j.biocel.2008.02.011

Baron, C. S., Kester, L., Klaus, A., Boisset, J.-C., Thambyrajah, R., Yvernogeau, L., Kouskoff, V., Lacaud, G., van Oudenaarden, A. and Robin, C. (2018). Single-cell transcriptomics reveal the dynamic of haematopoietic stem cell production in the aorta. *Nat. Commun.* **9**, 2517. doi:10.1038/s41467-018-04893-3

Ben Shoham, A., Malkinson, G., Krief, S., Shwartz, Y., Ely, Y., Ferrara, N., Yaniv, K. and Zelzer, E. (2012). S1P1 inhibits sprouting angiogenesis during vascular development. *Development* **139**, 3859-3869. doi:10.1242/dev.078550

Butler, A., Hoffman, P., Smibert, P., Papalexi, E. and Satija, R. (2018). Integrating single-cell transcriptomic data across different conditions, technologies, and species. *Nat. Biotechnol.* **36**, 411-420. doi:10.1038/nbt.4096

Camoretti-Mercado, B., Forsythe, S. M., LeBeau, M. M., Espinosa, R., III, Vieira, J. E., Halayko, A. J., Willadsen, S., Kurtz, B., Ober, C., Evans, G. A. et al. (1998). Expression and cytogenetic localization of the human SM22 gene (TAGLN). *Genomics* **49**, 452-457. doi:10.1006/geno.1998.5267

Carmeliet, P., Ferreira, V., Breier, G., Pollefeyt, S., Kieckens, L., Gertsenstein, M., Fahrig, M., Vandenhoeck, A., Harpal, K., Eberhardt, C. et al. (1996). Abnormal blood vessel development and lethality in embryos lacking a single VEGF allele. *Nature* **380**, 435-439. doi:10.1038/380435a0

Cevallos, M., Riha, G. M., Wang, X., Yang, H., Yan, S., Li, M., Chai, H., Yao, Q. and Chen, C. (2006). Cyclic strain induces expression of specific smooth muscle cell markers in human endothelial cells. *Differentiation* **74**, 552-561. doi:10.1111/j.1432-0436.2006.00089.x

Chai, J. Y., Jones, M. K. and Tarnawski, A. S. (2004). Serum response factor is a critical requirment for VEGF signaling in endothelial cells and VEGF-induced angiogenesis. *FASEB J.* **18**, 1264. doi:10.1096/fj.03-1232fje

Choi, K. J., Nam, J.-K., Kim, J.-H., Choi, S.-H. and Lee, Y.-J. (2020). Endothelial-to-mesenchymal transition in anticancer therapy and normal tissue damage. *Exp. Mol. Med.* **52**, 781-792. doi:10.1038/s12276-020-0439-4

Conway, E. M., Collen, D. and Carmeliet, P. (2001). Molecular mechanisms of blood vessel growth. *Cardiovasc. Res.* **49**, 507-521. doi:10.1016/S0008-6363(00)00281-9

De Bock, K., Georgiadou, M. and Carmeliet, P. (2013). Role of endothelial cell metabolism in vessel sprouting. *Cell Metab.* **18**, 634-647. doi:10.1016/j.cmet.2013.08.001

De Val, S., Chi, N. C., Meadows, S. M., Minovitsky, S., Anderson, J. P., Harris, I. S., Ehlers, M. L., Agarwal, P., Visel, A., Xu, S.-M. et al. (2008). Combinatorial regulation of endothelial gene expression by ets and forkhead transcription factors. *Cell* **135**, 1053-1064. doi:10.1016/j.cell.2008.10.049

Du, K. L., Ip, H. S., Li, J., Chen, M., Dandre, F., Yu, W., Lu, M. M., Owens, G. K. and Parmacek, M. S. (2003). Myocardin is a critical serum response factor cofactor in the transcriptional program regulating smooth muscle cell differentiation. *Mol. Cell. Biol.* **23**, 2425-2437. doi:10.1128/MCB.23.7.2425-2437.2003

Ferrara, N., Carver-Moore, K., Chen, H., Dowd, M., Lu, L., O'Shea, K. S., Powell-Braxton, L., Hillan, K. J. and Moore, M. W. (1996). Heterozygous embryonic lethality induced by targeted inactivation of the VEGF gene. *Nature* **380**, 439-442. doi:10.1038/380439a0

Frid, M. G., Kale, V. A. and Stenmark, K. R. (2002). Mature vascular endothelium can give rise to smooth muscle cells via endothelial-mesenchymal transdifferentiation: in vitro analysis. *Circ. Res.* **90**, 1189-1196. doi:10.1161/01.RES.0000021432.70309.28

Fu, Y., Liu, H. W., Forsythe, S. M., Kogut, P., McConville, J. F., Halayko, A. J., Camoretti-Mercado, B. and Solway, J. (2000). Mutagenesis analysis of human SM22: characterization of actin binding. *J. Appl. Physiol.* **89**, 1985-1990. doi:10.1152/jappl.2000.89.5.1985

Furuyama, T., Kitayama, K., Shimoda, Y., Ogawa, M., Sone, K., Yoshida-Araki, K., Hisatsune, H., Nishikawa, S., Nakayama, K., Nakayama, K. et al. (2004). Abnormal angiogenesis in Foxo1 (Fkhr)-deficient mice. *J. Biol. Chem.* **279**, 34741-34749. doi:10.1074/jbc.M314214200

Geudens, I. and Gerhardt, H. (2011). Coordinating cell behaviour during blood vessel formation. *Development* **138**, 4569-4583. doi:10.1242/dev.062323

Gimona, M., Kaverina, I., Resch, G. P., Vignal, E. and Burgstaller, G. (2003). Calponin repeats regulate actin filament stability and formation of podosomes in smooth muscle cells. *Mol. Biol. Cell* **14**, 2482-2491. doi:10.1091/mbc.e02-11-0743

Guo, R., Sakamoto, H., Sugiura, S. and Ogawa, M. (2007). Endothelial cell motility is compatible with junctional integrity. *J. Cell. Physiol.* **211**, 327-335. doi:10.1002/jcp.20937

Hall, S. M., Hislop, A. A. and Haworth, S. G. (2002). Origin, differentiation, and maturation of human pulmonary veins. *Am. J. Respir. Cell Mol. Biol.* **26**, 333-340. doi:10.1165/ajrcmb.26.3.4698

Hautmann, M. B., Adam, P. J. and Owens, G. K. (1999). Similarities and differences in smooth muscle alpha-actin induction by TGF-β in smooth muscle versus non-smooth muscle cells. *Arterioscler. Thromb. Vasc. Biol.* **19**, 2049-2058. doi:10.1161/01.ATV.19.9.2049

Hirashima, M., Kataoka, H., Nishikawa, S., Matsuyoshi, N. and Nishikawa, S.-I. (1999). Maturation of embryonic stem cells into endothelial cells in an in vitro model of vasculogenesis. *Blood* **93**, 1253-1263. doi:10.1182/blood.V93.4.1253

Jin, H., Cheng, X., Pei, Y., Fu, J., Lyu, Z., Peng, H., Yao, Q., Jiang, Y., Luo, L. and Zhuo, H. (2016). Identification and verification of transgelin-2 as a potential biomarker of tumor-derived lung-cancer endothelial cells by comparative proteomics. *J. Proteomics* **136**, 77-88. doi:10.1016/j.jprot.2015.12.012

Kataoka, H., Takakura, N., Nishikawa, S., Tsuchida, K., Kodama, H., Kunisada, T., Risau, W., Kita, T. and Nishikawa, S.-I. (1997). Expressions of PDGF receptor alpha, c-Kit and Flk1 genes clustering in mouse chromosome 5 define distinct subsets of nascent mesodermal cells. *Dev. Growth Differ.* **39**, 729-740. doi:10.1046/j.1440-169X.1997.t01-5-00009.x

Kim, S., Ip, H. S., Lu, M. M., Clendenin, C. and Parmacek, M. S. (1997). A serum response factor-dependent transcriptional regulatory program identifies distinct smooth muscle cell sublineages. *Mol. Cell. Biol.* **17**, 2266-2278. doi:10.1128/MCB.17.4.2266

Kim, H.-R., Kwon, M.-S., Lee, S., Mun, Y., Lee, K.-S., Kim, C.-H., Na, B.-R., Kim, B. N. R., Piragyte, I., Lee, H.-S. et al. (2018). TAGLN2 polymerizes G-actin in a low ionic state but blocks Arp2/3-nucleated actin branching in physiological conditions. *Sci. Rep.* **8**, 5503. doi:10.1038/s41598-018-23816-2

Kodama, H., Nose, M., Niida, S., Nishikawa, S. and Nishikawa, S. (1994). Involvement of the c-kit receptor in the adhesion of hematopoietic stem cells to stromal cells. *Exp. Hematol.* **22**, 979-984.

Lawson, D., Harrison, M. and Shapland, C. (1997). Fibroblast transgelin and smooth muscle SM22α are the same protein, the expression of which is down-regulated in many cell lines. *Cell Motil. Cytoskeleton* **38**, 250-257. doi:10.1002/(SICI)1097-0169(1997)38:3<250::AID-CM3>3.0.CO;2-9

Lees-Miller, J. P., Heeley, D. H. and Smillie, L. B. (1987). An abundant and novel protein of 22 kDa (SM22) is widely distributed in smooth muscles. Purification from bovine aorta. *Biochem. J.* **244**, 705-709. doi:10.1042/bj2440705

Lew, Z.-X., Zhou, H.-M., Fang, Y.-Y., Ye, Z., Zhong, W., Yang, X.-Y., Yu, Z., Chen, D.-Y., Luo, S.-M., Chen, L.-F. et al. (2020). Transgelin interacts with PARP1 in human colon cancer cells. *Cancer Cell Int.* **20**, 366. doi:10.1186/s12935-020-01461-y

Li, L., Miano, J. M., Cserjesi, P. and Olson, E. N. (1996). SM22α, a marker of adult smooth muscle, is expressed in multiple myogenic lineages during embryogenesis. *Circ. Res.* **78**, 188-195. doi:10.1161/01.RES.78.2.188

Liebner, S., Cattelino, A., Gallini, R., Rudini, N., Iurlaro, M., Piccolo, S. and Dejana, E. (2004). Beta-catenin is required for endothelial-mesenchymal transformation during heart cushion development in the mouse. *J. Cell Biol.* **166**, 359-367. doi:10.1083/jcb.200403050

Mack, C. P. (2011). Signaling mechanisms that regulate smooth muscle cell differentiation. *Arterioscler. Thromb. Vasc. Biol.* **31**, 1495-1505. doi:10.1161/ATVBAHA.110.221135

Matsukawa, M., Sakamoto, H., Kawasuji, M., Furuyama, T. and Ogawa, M. (2009). Different roles of Foxo1 and Foxo3 in the control of endothelial cell morphology. *Genes Cells* **14**, 1167-1181. doi:10.1111/j.1365-2443.2009.01343.x

Matsuyoshi, N., Toda, K., Horiguchi, Y., Tanaka, T., Nakagawa, S., Takeichi, M. and Imamura, S. (1997). In vivo evidence of the critical role of cadherin-5 in murine vascular integrity. *Proc. Assoc. Am. Physicians* **109**, 362-371.

Merks, R. M. H., Brodsky, S. V., Goligorksy, M. S., Newman, S. A. and Glazier, J. A. (2006). Cell elongation is key to in silico replication of in vitro vasculogenesis and subsequent remodeling. *Dev. Biol.* **289**, 44-54. doi:10.1016/j.ydbio.2005.10.003

Nakahara, M., Tateyama, H., Araki, M., Nakagata, N., Yamamura, K. and Araki, K. (2013). Gene-trap mutagenesis using Mol/MSM-1 embryonic stem cells from MSM/Ms mice. *Mamm. Genome* **24**, 228-239. doi:10.1007/s00335-013-9452-4

Nishida, W., Nakamura, M., Mori, S., Takahashi, M., Ohkawa, Y., Tadokoro, S., Yoshida, K., Hiwada, K., Hayashi, K. and Sobue, K. (2002). A triad of serum response factor and the GATA and NK families governs the transcription of smooth and cardiac muscle genes. *J. Biol. Chem.* **277**, 7308-7317. doi:10.1074/jbc.M111824200

Niwa, H., Yamamura, K.-I. and Miyazaki, J.-I. (1991). Efficient selection for high-expression transfectants with a novel eukaryotic vector. *Gene* **108**, 193-199. doi:10.1016/0378-1119(91)90434-D

Owens, G. K., Kumar, M. S. and Wamhoff, B. R. (2004). Molecular regulation of vascular smooth muscle cell differentiation in development and disease. *Physiol. Rev.* **84**, 767-801. doi:10.1152/physrev.00041.2003

Park, S.-H., Sakamoto, H., Tsuji-Tamura, K., Furuyama, T. and Ogawa, M. (2009). Foxo1 is essential for in vitro vascular formation from embryonic stem cells. *Biochem. Biophys. Res. Commun.* **390**, 861-866. doi:10.1016/j.bbrc.2009.10.063

Qiu, P., Feng, X. H. and Li, L. (2003). Interaction of Smad3 and SRF-associated complex mediates TGF-β1 signals to regulate SM22 transcription during myofibroblast differentiation. *J. Mol. Cell. Cardiol.* **35**, 1407-1420. doi:10.1016/j.yjmcc.2003.09.002

Qutub, A. A. and Popel, A. S. (2009). Elongation, proliferation & migration differentiate endothelial cell phenotypes and determine capillary sprouting. *BMC Syst. Biol.* **3**, 13. doi:10.1186/1752-0509-3-13

Shapland, C., Lowings, P. and Lawson, D. (1988). Identification of new actin-associated polypeptides that are modified by viral transformation and changes in cell shape. *J. Cell Biol.* **107**, 153-161. doi:10.1083/jcb.107.1.153

Shapland, C., Hsuan, J. J., Totty, N. F. and Lawson, D. (1993). Purification and properties of transgelin: a transformation and shape change sensitive actin-gelling protein. *J. Cell Biol.* **121**, 1065-1073. doi:10.1083/jcb.121.5.1065

Stuart, T., Butler, A., Hoffman, P., Hafemeister, C., Papalexi, E., Mauck, W. M., III, Hao, Y., Stoeckius, M., Smibert, P. and Satija, R. (2019). Comprehensive integration of single-cell data. *Cell* **177**, 1888-1902.e21. doi:10.1016/j.cell.2019.05.031

The Gene Ontology Consortium. (2019). The Gene Ontology Resource: 20 years and still GOing strong. *Nucleic Acids Res.* **47**, D330-D338. doi:10.1093/nar/gky1055

Tsuji-Tamura, K. and Ogawa, M. (2016). Inhibition of the PI3K-Akt and mTORC1 signaling pathways promotes the elongation of vascular endothelial cells. *J. Cell Sci.* **129**, 1165-1178. doi:10.1242/jcs.178434

Tsuji-Tamura, K. and Ogawa, M. (2018a). Dual inhibition of mTORC1 and mTORC2 perturbs cytoskeletal organization and impairs endothelial cell elongation. *Biochem. Biophys. Res. Commun.* **497**, 326-331. doi:10.1016/j.bbrc.2018.02.080

Tsuji-Tamura, K. and Ogawa, M. (2018b). Morphology regulation in vascular endothelial cells. *Inflamm Regen* **38**, 25. doi:10.1186/s41232-018-0083-8

Tsuji-Tamura, K., Sakamoto, H. and Ogawa, M. (2011). ES cell differentiation as a model to study cell biological regulation of vascular development. In *Embryonic Stem Cells: The Hormonal Regulation of Pluripotency and Embryogenesis* (ed. C. S. Atwood), pp. 581-606. InTech.

Tsuji-Tamura, K., Sato, M., Fujita, M. and Tamura, M. (2020a). Glycine exerts dose-dependent biphasic effects on vascular development of zebrafish embryos. *Biochem. Biophys. Res. Commun.* **527**, 539-544. doi:10.1016/j.bbrc.2020.04.098

Tsuji-Tamura, K., Sato, M., Fujita, M. and Tamura, M. (2020b). The role of PI3K/Akt/mTOR signaling in dose-dependent biphasic effects of glycine on vascular

development. *Biochem. Biophys. Res. Commun.* **529**, 596-602. doi:10.1016/j.bbrc.2020.06.085

Varberg, K. M., Garretson, R. O., Blue, E. K., Chu, C., Gohn, C. R., Tu, W. and Haneline, L. S. (2018). Transgelin induces dysfunction of fetal endothelial colony-forming cells from gestational diabetic pregnancies. *Am. J. Physiol. Cell Physiol.* **315**, C502-C515. doi:10.1152/ajpcell.00137.2018

Wang, G., Yang, Q., Li, M., Zhang, Y., Cai, Y., Liang, X., Fu, Y., Xiao, Z., Zhou, M., Xie, Z. et al. (2019). Quantitative proteomic profiling of tumor-associated vascular endothelial cells in colorectal cancer. *Biol Open* **8**, bio042838. doi:10.1242/bio.042838

Yagi, T., Tokunaga, T., Furuta, Y., Nada, S., Yoshida, M., Tsukada, T., Saga, Y., Takeda, N., Ikawa, Y. and Aizawa, S. (1993). A novel ES cell-line, Tt2, with high germline-differentiating potency. *Anal. Biochem.* **214**, 70-76. doi:10.1006/abio.1993.1458

Yamashita, J., Itoh, H., Hirashima, M., Ogawa, M., Nishikawa, S.-I., Yurugi, T., Naito, M., Nakao, K. and Nishikawa, S. (2000). Flk1-positive cells derived from embryonic stem cells serve as vascular progenitors. *Nature* **408**, 92-96. doi:10.1038/35040568

Yokomizo, T. and Dzierzak, E. (2010). Three-dimensional cartography of hematopoietic clusters in the vasculature of whole mouse embryos. *Development* **137**, 3651-3661. doi:10.1242/dev.051094

Zeidan, A., Swärd, K., Nordström, I., Ekblad, E., Zhang, J. C. L., Parmacek, M. S. and Hellstrand, P. (2004). Ablation of SM22α decreases contractility and actin contents of mouse vascular smooth muscle. *FEBS Lett.* **562**, 141-146. doi:10.1016/S0014-5793(04)00220-0

Zeisberg, E. M., Tarnavski, O., Zeisberg, M., Dorfman, A. L., McMullen, J. R., Gustafsson, E., Chandraker, A., Yuan, X., Pu, W. T., Roberts, A. B. et al. (2007). Endothelial-to-mesenchymal transition contributes to cardiac fibrosis. *Nat. Med.* **13**, 952-961. doi:10.1038/nm1613

Zhang, J. C. L., Kim, S., Helmke, B. P., Yu, W. W., Du, K. L., Lu, M. M., Strobeck, M., Yu, Q.-C. and Parmacek, M. S. (2001). Analysis of SM22α-deficient mice reveals unanticipated insights into smooth muscle cell differentiation and function. *Mol. Cell. Biol.* **21**, 1336-1344. doi:10.1128/MCB.2001.21.4.1336-1344.2001

Zhong, W. L., Hou, H. Q., Liu, T. Y., Su, S., Xi, X. N., Liao, Y. S., Xie, R. X., Jin, G., Liu, X., Zhu, L. P. et al. (2020). Cartilage Oligomeric Matrix Protein promotes epithelial-mesenchymal transition by interacting with Transgelin in Colorectal Cancer. *Theranostics* **10**, 8790-8806. doi:10.7150/thno.44456

Zhou, H. M., Li, L., Xie, W. R., Wu, L. H., Lin, Y. and He, X. X. (2020). TAGLN and High-mobility Group AT-Hook 2 (HMGA2) complex regulates TGF-β-induced colorectal cancer metastasis. *Oncotarget. Ther.* **13**, 10489-10498. doi:10.2147/OTT.S263090

Zovein, A. C., Hofmann, J. J., Lynch, M., French, W. J., Turlo, K. A., Yang, Y., Becker, M. S., Zanetta, L., Dejana, E., Gasson, J. C. et al. (2008). Fate tracing reveals the endothelial origin of hematopoietic stem cells. *Cell Stem Cell* **3**, 625-636. doi:10.1016/j.stem.2008.09.018

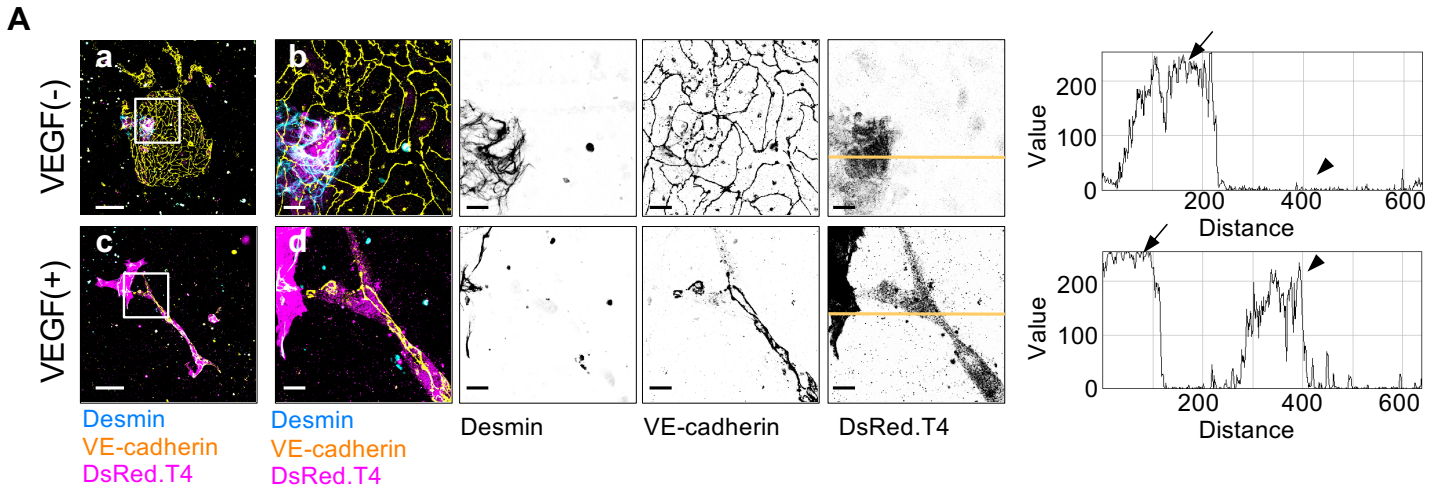

Figure S1. The *Tagln* promoter is activated in ECs stimulated with VEGF

KDR$^+$ cells induced from F10-EGFP/Tagln-DsRed.T4 ESCs were cultured on an OP9 cell layer for four days with or without addition of VEGF (10 ng/ml). We obtained z-stack confocal images of cultures after fixation and immunostaining. (A) Immunostaining of desmin (cyan), VE-cadherin (yellow) and DsRed.T4 (magenta). Multiple or individual channels are shown as merged or black-white inverted images, respectively. Panels (b) and (d) show higher magnifications of the boxed area in panels (a) and (c), respectively. Scale bars indicate 100 µm (a and c) or 20 µm (b and d). The right panels show the fluorescence intensity profiles along each yellow line in the DsRed.T4 image. Arrows and arrowheads indicate the peaks of SMCs and ECs, respectively. Similar results were obtained in three independent experiments using two clones. (B) ECs were categorized into the two types of EC shape: cobblestone (type cob) and elongated (type elong), and scored as either Desmin+ or Desmin−. The proportion of Desmin− and Desmin+ ECs with the two types of EC shape are shown. The total number of ECs of each shape for the two VEGF treatments, observed across three independent experiments using different clones, is indicated in the brackets.

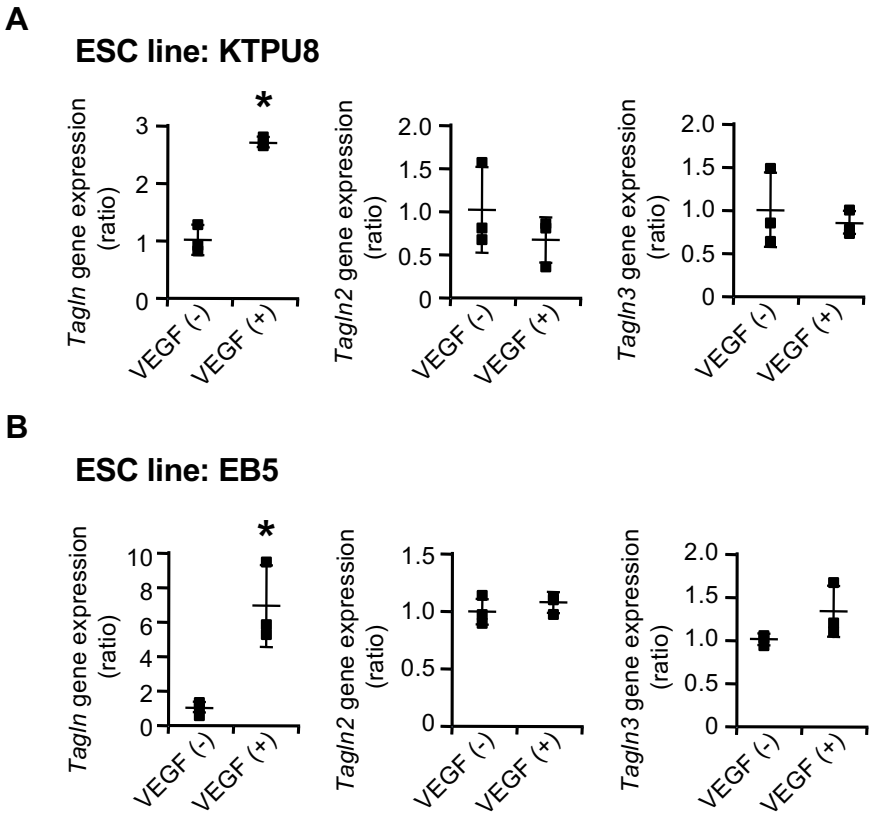

Figure S2. Expressions of *Tagln* isoforms in ECs derived from ESCs

KDR^{+} cells induced from two mouse ESC lines, KTPU8 and EB5, were cultured on an OP9 cell layer with or without the addition of VEGF (10 ng/ml). After four days, CD45^{-} VE-cadherin^{+} CD31^{+} KDR^{+} ECs were purified. (A and B) Expressions of the *Tagln, Tagln2 and Tagln3* genes in ECs derived from KTPU8 (A) and EB5 (B) were quantified using real-time quantitative PCR. Expression levels were normalized to *B2m*. Data is presented as a ratio relative to the VEGF (-) control (mean ± SD, n = 3 from three independent experiments). The Data were analyzed using F-test, followed by a two-tailed t-test (* $p < 0.05$).

A

***TAGLN* (WT)**

GGATCATAGTGCAGTGTGGCCCTGATGTGGGC**CGCCCAGACCGTGGGCGCTTGGG**CTTCCAGGTCTGGC

***SM22* (8-bp deletion)**

GGATCATAGTGCAGTGTGGCCCTGATGTGGGC**CGCCCAGACCGT**-------- **GGG**CTTCCAGGTCTGGC

***TAGLN2* (WT)**

CAGATCCTGATCCAGTGGATCACCACCCAGTG**CCGAAAGGATGTGGGCCGGCCCC**AGCCTGGACGCGAG

***Tagln2* (32-bp deletion)**

CAGATCCTGATCCAG---------- **CCGGCCCC**AGCCTGGACGCGAG

***TAGLN3* (WT)**

GATGCGGACCTGGAGAACAAGCTGGTGGACTG**GATCATCCTGCAGTGCGCCG**AGGACATAGAGCACCCG

***Tagln3* (10-bp deletion)**

GATGCGGACCTGGAGAACAAGCTGGTGGACTG**GATCATCCTGCAGTGCG**---------- AGAGCACCCG

B

***TAGLN* (8-bp deletion)**

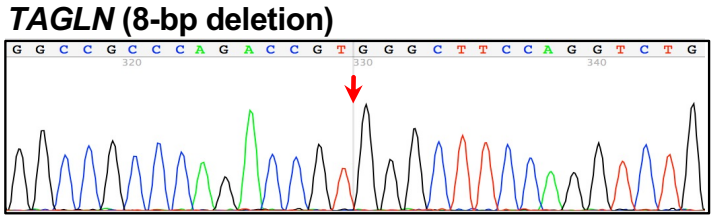

***TAGLN2* (32-bp deletion)**

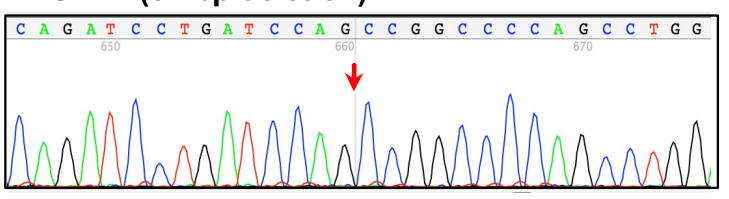

***TAGLN3* (10-bp deletion)**

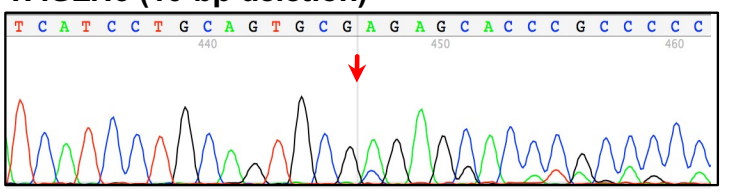

C

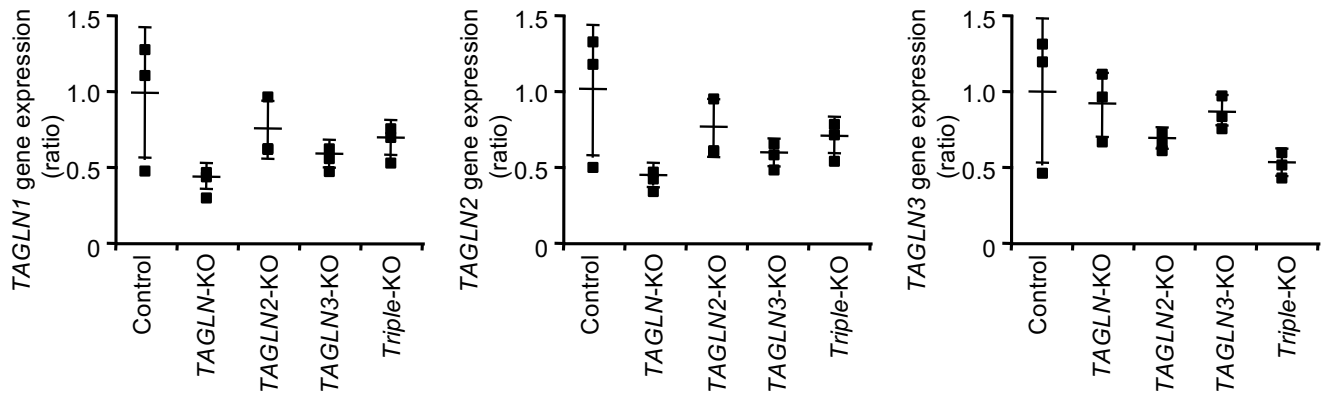

Figure S3. CRISPR/Cas9-mediated mutagenesis of the *TAGLN* isoforms

(A) Sequences of wild type (WT) and the representative mutations at target sites of genome editing in *TAGLN*, *TAGLN2* and *TAGLN3* genes. The target sequence and the PAM region are indicated in blue and red, respectively. Dashes (-) indicate deletions. (B) Nucleotide peaks of the representative mutated sequence at target sites of *TAGLN*, *TAGLN2* and *TAGLN3* genes. Red arrows indicate the location of mutations. (C) HUVECs were genetically edited in *TAGLN*, *TAGLN2* and *TAGLN3* genes with CRISPR/Cas9 system, which indicated as follows: *TAGLN*, *TAGLN2*, *TAGLN3* single-KO (KO), *TAGLN* isoforms triple-KO (triple-KO). The mRNA expression level of *TAGLN* isoforms was determined using real-time quantitative PCR analysis. Data were normalized to *B2M*, and are presented as fold change relative to the control (mean ± SD, n = 3 from three independent experiments). Data were analyzed using Tukey's test. No significant difference was found. These primers used for *TAGLN* isoforms target the downstream regions of CRISPR targeting sites in each gene. The amplification of fragments was not affected by each gene knockout.

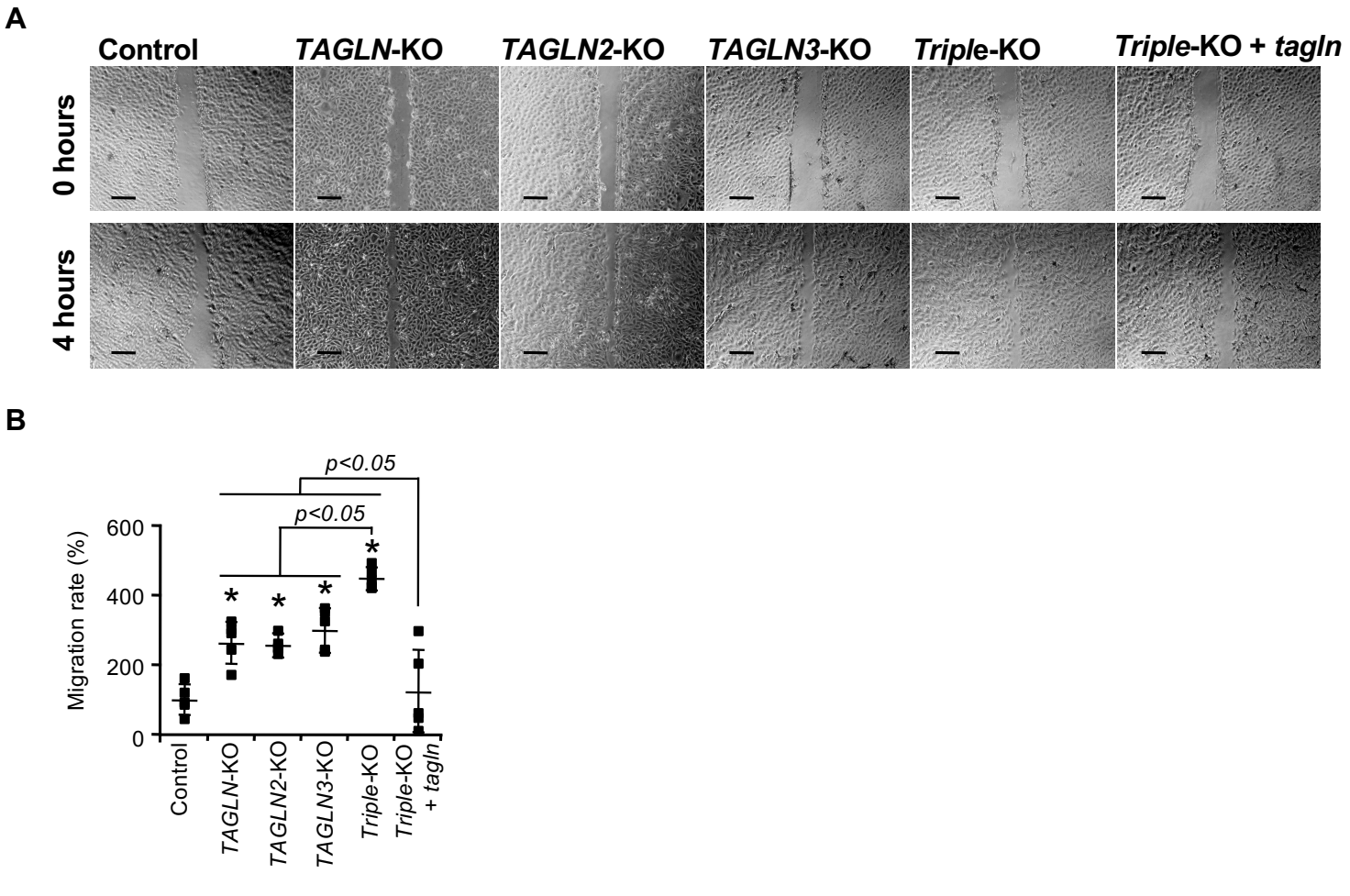

Figure S4. Single and triple-knockout of *TAGLN* isoforms promotes migration of ECs.

HUVECs were genetically edited in *TAGLN*, *TAGLN2* and *TAGLN3* genes with CRISPR/Cas9 system, and applied to rescue expression of zebrafish *tagln*, which indicated as follows: *TAGLN*, *TAGLN2*, *TAGLN3* single-KO (KO), *TAGLN* isoforms triple-KO (triple-KO), and *tagln*-expression-rescued triple-KO (triple-KO + *tagln*). The cell monolayers were scratched using a universal cell scraper. (A) Phase-contrast images at 0 and 4 hours after scratch generation. Scale bars indicate 200 μm. Similar results were obtained in five independent experiments. (B) The migration rate are presented as the mean ± SD (n = 5 from five independent experiments). Data were analyzed using Tukey's test (* $p < 0.05$ compared with the control).

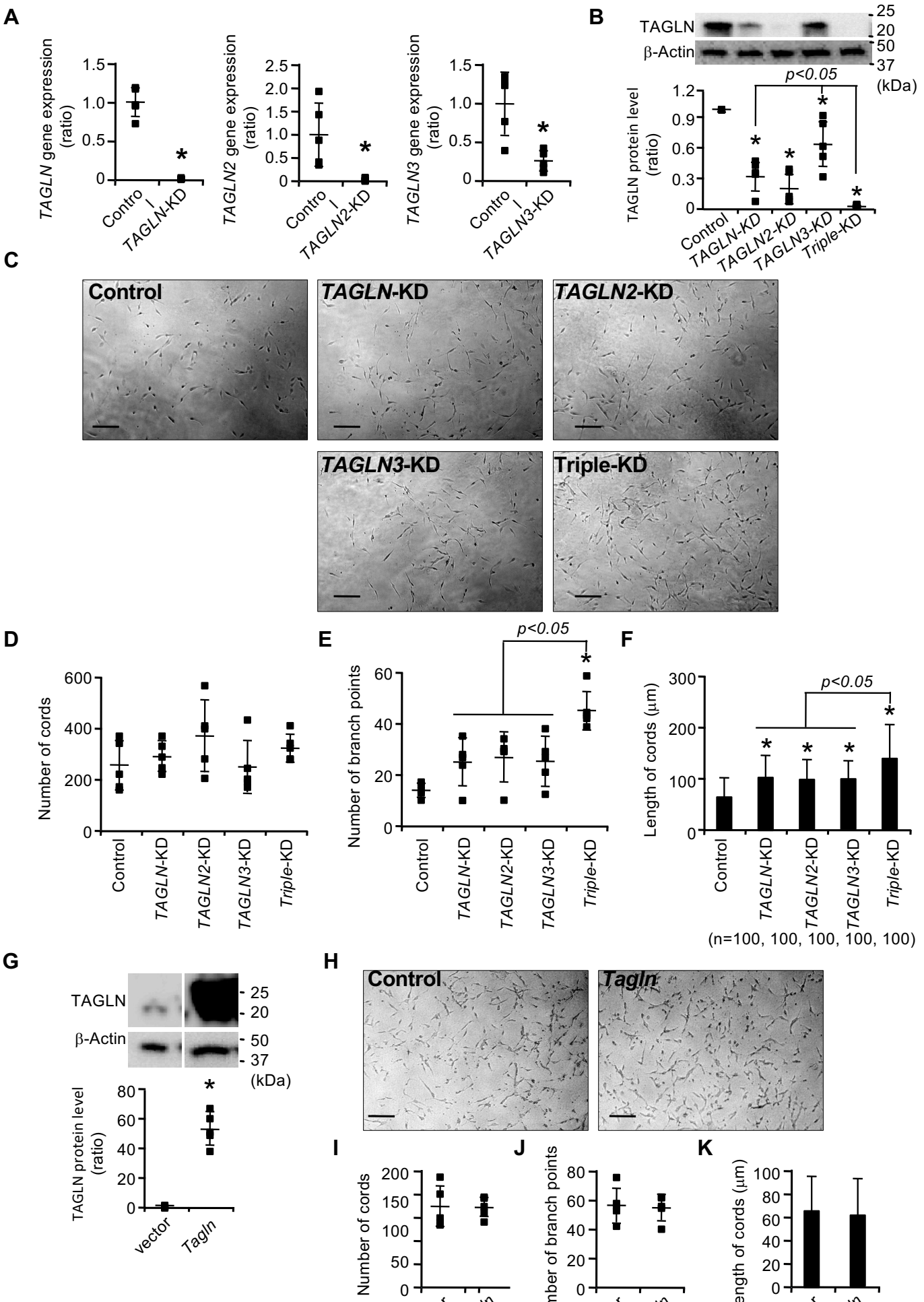

Figure S5. Single and triple-knockdown of *TAGLN* isoforms causes excessive cord-like structure formation
(A-F) HUVECs were transfected with a single siRNA targeting *TAGLN, TAGLN2* or *TAGLN3* (44 pg), a mixture of *TAGLN* isoforms siRNAs (44 pg each, total 132 pg), or control siRNA (132 pg), which indicated as follows: *TAGLN*, *TAGLN2*, *TAGLN3* single-knockdown (KD), and *TAGLN* isoforms triple-KD (triple-KD). (A) The mRNA expression level of *TAGLN* isoforms was determined using real-time quantitative PCR analysis. Data were normalized to *B2M,* and are presented as fold change relative to the control (mean ± SD, n = 5 from five independent experiments). The data were analyzed using F-test, followed by a two-tailed t-test (* $p < 0.05$). (B) Western blot analysis with antibodies against the TAGLN protein (ab14106, Abcam). (Upper) Western blot images. β-Actin protein was used as an internal control. Similar results were obtained in five independent experiments. (Lower) Expression levels were normalized to β-Actin. Data are presented as a ratio relative to the control group (mean ± SD, n = 5 from five independent experiments). The data were analyzed using Tukey's test (* $p < 0.05$ compared with the control group). (C–F) siRNA-transfected HUVECs were grown in 3D sandwich culture in the presence of VEGF (10 ng/ml) for one day. (C) Phase-contrast images. Scale bars indicate 200 μm. Similar results were obtained in three independent experiments. (D and E) The number of cord-like structure (D) and branch points (E) per field is presented as the mean ± SD (n = 5 fields per group). The data were analyzed using Tukey's test (* $p < 0.05$ compared with the control). (F) The length of the cord-like structure is presented as the mean ± SD. The total number of cords examined is indicated in the brackets. The data were analyzed using Tukey's test (* $p < 0.05$ compared with the control). (G-K) HUVECs were transfected with pCAG-Ipuro expressing mouse *Tagln* or pCAG-Ipuro vector. (G) Western blot analysis with antibodies against the TAGLN protein (ab14106, Abcam). (Upper) Western blot images. β-Actin protein was used as an internal control. Similar results were obtained in five independent experiments. (Lower) Expression levels were normalized to β-Actin. Data are presented as a ratio relative to the control group (mean ± SD, n = 5 from five independent experiments). The data were analyzed using F-test, followed by a two-tailed t-test (* $p < 0.05$). (H–K) *Tagln*-transfected HUVECs were grown in 3D sandwich culture in the
presence of VEGF (10 ng/ml) for one day. (H) Phase-contrast images. Scale bars indicate 200 μm. Similar results were obtained in three independent experiments. (I and J) The number of cord-like structure (I) and branch points (J) per field is presented as the mean ± SD (n = 5 fields per group). The data were analyzed using F-test, followed by a two-tailed t-test. (K) The length of the cord-like structure is presented as the mean ± SD. The total number of cords examined is indicated in the brackets. The data were analyzed using F-test, followed by a two-tailed t-test.

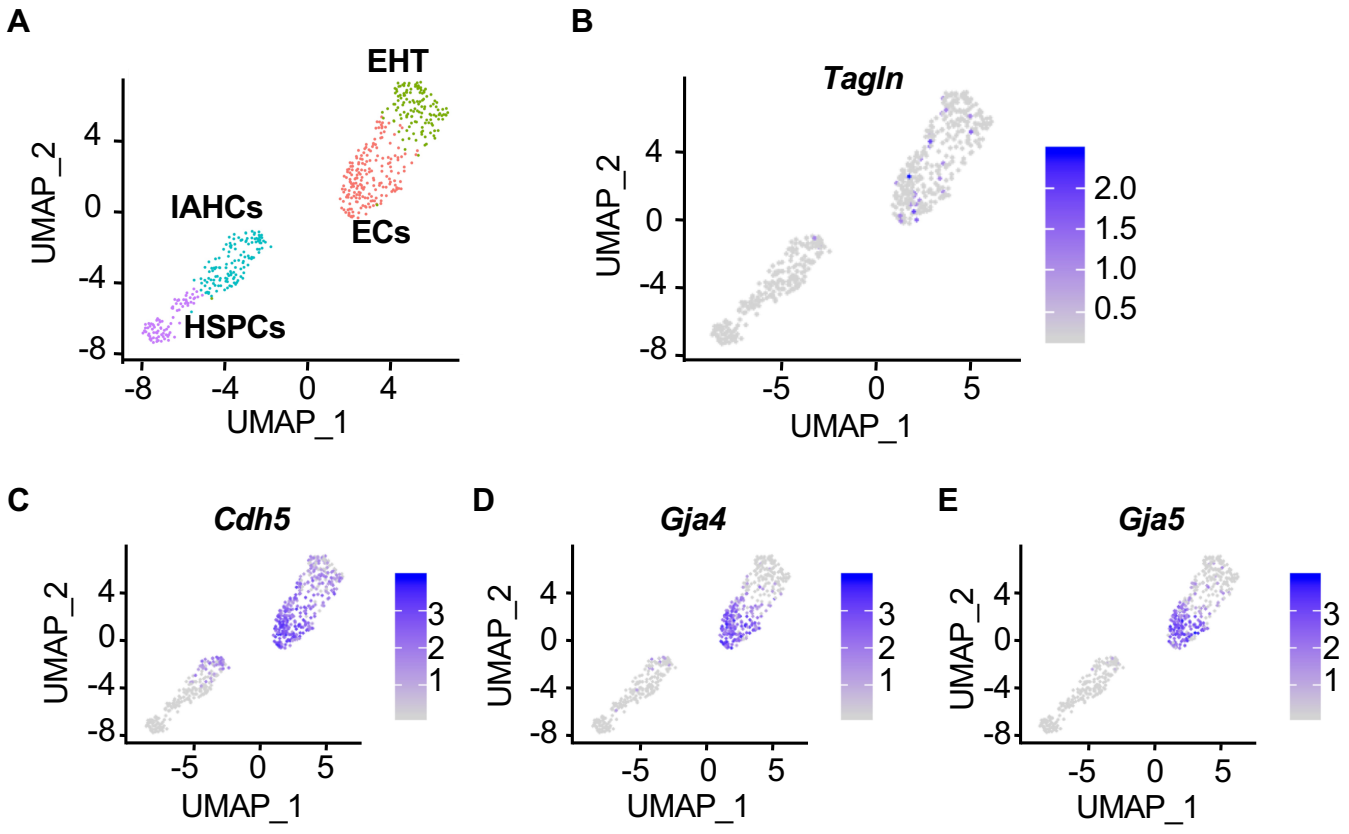

Figure S6. *Tagln*-expressing cells are detected in the EC cluster from embryonic aortas

Analysis of a single cell RNA-seq dataset of E10.5 mouse embryonic aortas. (A) Canonical cell markers were used to label clusters by cell identity based on the previous report (Baron et al., 2018) as represented in the UMAP plot. ECs: endothelial cells, EHT: endothelial-to-hematopoietic transition, IAHCs: intra-aortic hematopoietic clusters, HSPCs: hematopoietic stem and progenitor cells. (B, C, D and E) The feature plot shows the expression of *Tagln* (B) and endothelial cell markers, *Cdh5* (C), *Gja4* (D) and *Gja5* (E).

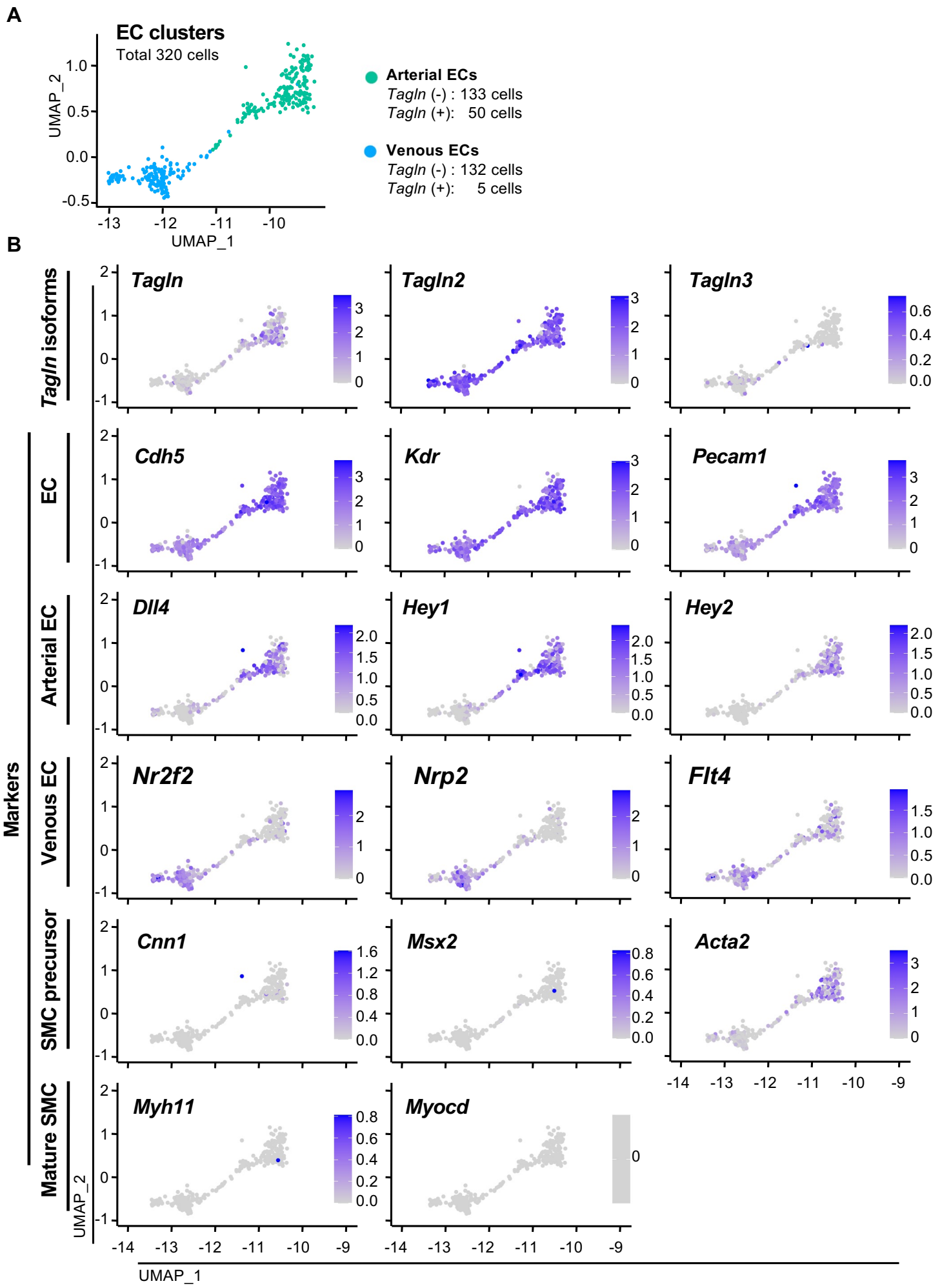
A
EC clusters
Total 320 cells
UMAP_2
UMAP_1
Arterial ECs
Tagln (-) : 133 cells
Tagln (+): 50 cells
Venous ECs
Tagln (-) : 132 cells
Tagln (+): 5 cells
B
Markers
Tagln isoforms
EC
Arterial EC
Venous EC
SMC precursor
Mature SMC
Tagln
Tagln2
Tagln3
Cdh5
Kdr
Pecam1
Dll4
Hey1
Hey2
Nr2f2
Nrp2
Flt4
Cnn1
Msx2
Acta2
Myh11
Myocd
UMAP_2
UMAP_1

Figure S7. *Tagln*-expressing cells are detected in the arterial and venous EC clusters

Analysis of a single cell RNA-seq dataset of the AGM region and the FL of an E10.5 mouse embryo. (A) Arterial and venous EC clusters in the total EC cluster. The green dots show arterial ECs. The blue dots show venous ECs. (B) The feature plots show the expression of *Tagln* isoforms, and markers for EC, arterial EC, venous EC, SMC precursor and mature SMC. Canonical cell markers were based on the previous reports (Chang et al., 2012) (for a review, see (Heinke et al., 2012)).

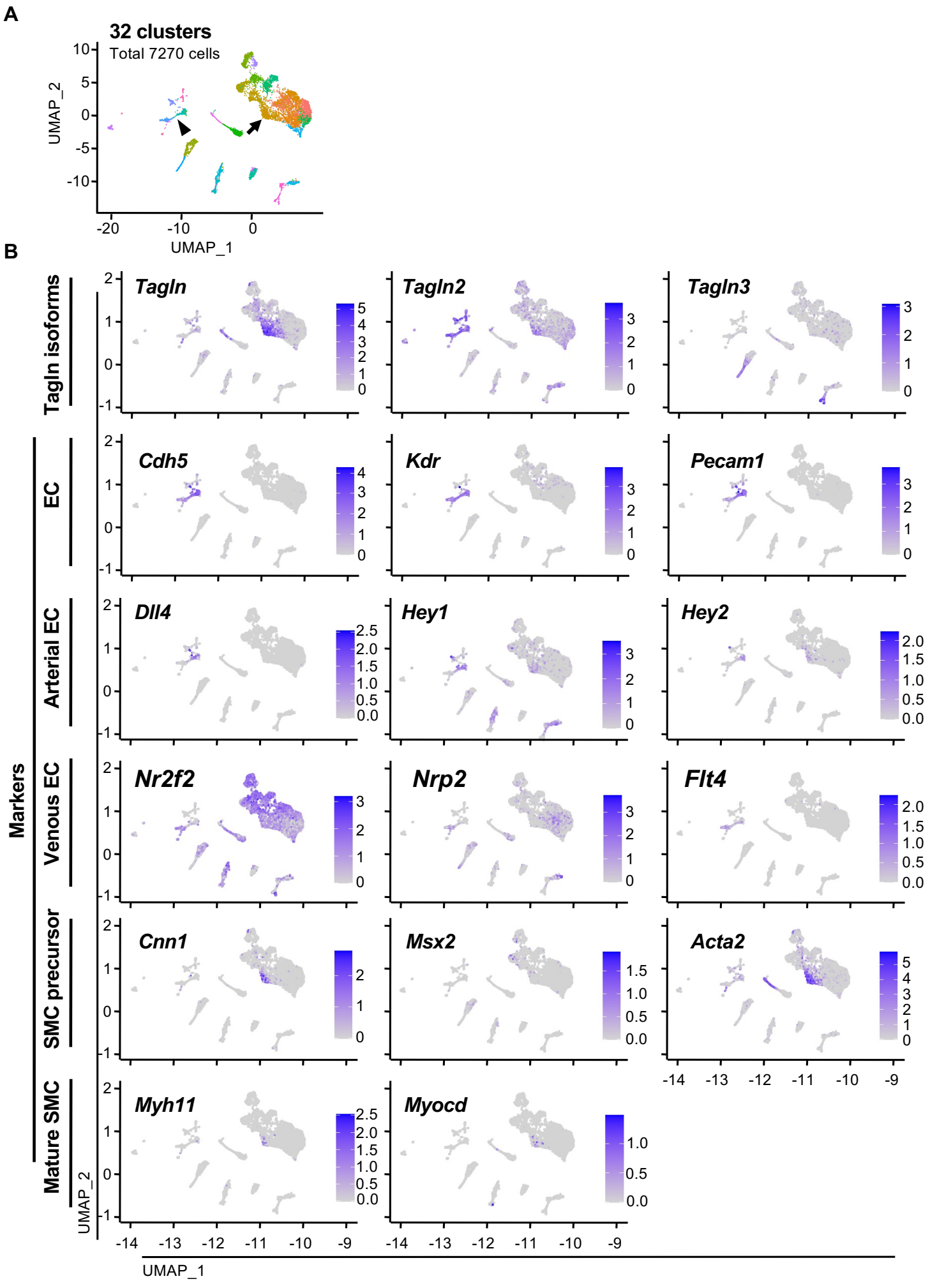

Figure S8. *Tagln* -expressing cells are detected in both EC and SMC clusters. Analysis of a single cell RNA-seq dataset of the AGM region and the FL of an E10.5 mouse embryo. (A) Total 32 clusters. The arrowhead points to the total EC cluster shown in Supplementary figure 7. The arrow points to the SMC cluster. (B) The feature plots show the expression of *Tagln* isoforms, and markers for EC, arterial EC, venous EC, SMC precursor and mature SMC.

Table S1. List of genes highly expressed in *Tagln* -positive ECs in embryonic aortas

gene	avg_logFC
Tagln	1.298254105
Acta2	1.252795771
Eln	1.225094955
Fbln5	0.652144013
Car4	0.635177264
Lamc1	0.542729891
Reg3b	0.53645699
Pdlim3	0.490619397
Slc2a1	0.488762541
Igfbp7	0.472637949
Lsr	0.463220813
Myl12a	0.456294191
Wbp1	0.447633409
Hmg20a	0.440111165
Tpm1	0.440099826
St3gal5	0.435698182
Mcts1	0.43517988
Fbln2	0.431716937
Tm4sf1	0.429455732
Tie1	0.425069231
Col3a1	0.424927296
Kras	0.423854609
Cdkn1c	0.422729154
Chtf8	0.419118954
Jam3	0.416155381
Hipk3	0.409065587
Rtf1	0.400691343
Mrpl4	0.398818005
Ash2l	0.396356419
8430408G22Rik	0.396146909
Ist1	0.390825899
Wdr26	0.387434777

gene	avg_logFC
Slc22a23	0.386482734
Trim27	0.384438805
Impdh1	0.379036697
Rnf215	0.379026475
Phf14	0.377817685
Tgfb1i1	0.375543426
Drap1	0.374364313
Dtx2	0.371840362
Zc3h7a	0.371799869
Btg2	0.371518371
Dnajb4	0.367692871
Gata2	0.365689289
Poc1b	0.363878479
Dnajc3	0.362934149
Mrpl51	0.362207936
Myadm	0.362163692
Flna	0.361683614
S100a11	0.360985408
Frmd8	0.360441406
Rai14	0.359601271
Tmem2	0.359134366
Pan3	0.358562311
9530068E07Rik	0.357045698
Phf20l1	0.356027931
Slc31a1	0.353012216
Yipf6	0.35104851
Il15	0.351024636
Gns	0.350236307
Lsmd1	0.349790844
Qk	0.34419299
Golt1b	0.343473095
Riok2	0.342806516

gene	avg_logFC
Hsd17b10	0.34172693
Pbdc1	0.341083816
Prnd	0.341019554
Khdrbs3	0.339911471
Ensa	0.339244925
Galnt2	0.339067826
Unc5b	0.338496426
Fbxl20	0.338239246
Cacna1a	0.336892608
Pdhb	0.336789987
Csrp2	0.335267949
Chd6	0.334486059
Col4a1	0.332944567
Pnpla2	0.332778986
Urod	0.332622693
Itgb1	0.330644585
Scube1	0.330501609
Capn2	0.3298931
Bptf	0.32870413
Dcaf12l1	0.328407283
Hps5	0.328271059
Igf2r	0.32817896
Acvr1	0.327801119
Kdm2b	0.327784046
Rnasek	0.32716961
Pja2	0.326442668
Ajuba	0.325255251
Tnfaip2	0.325212424
Myo1c	0.323585563
Nfib	0.323081132
Rras	0.322059865

Table S2. List of gene ontology (OG) associated with genes in Supplementary table 1

GO biological process complete	Fold Enrichment	raw P-value	FDR
angiogenesis (GO:0001525)	7.06	0.0000065	0.020500
blood vessel morphogenesis (GO:0048514)	5.74	0.0000114	0.022400
tube morphogenesis (GO:0035239)	4.42	0.0000083	0.018800
head development (GO:0060322)	4.37	0.0000214	0.037500
tube development (GO:0035295)	4.21	0.0000012	0.019300
anatomical structure formation involved in morphogenesis (GO:0048646)	3.97	0.0000056	0.029700
anatomical structure morphogenesis (GO:0009653)	2.66	0.0000069	0.018200
cellular component organization (GO:0016043)	1.94	0.0000051	0.040100
cellular component organization or biogenesis (GO:0071840)	1.92	0.0000062	0.024300

Table S3. List of genes highly expressed in *Tagln*-positive ECs from AGM and FL

The asterisks are the genes shown in supplementary table 1.

	gene	avg_logFC
*	Tagln	2.20949927
*	Acta2	1.7442024
	Actc1	1.06343492
*	Tpm1	0.91730392
	Myl9	0.88662588
*	Btg2	0.61183573
	Lgals1	0.52584705
	Prdx4	0.52543552
	Tmem100	0.515779
	Txnip	0.51104832
	Spon2	0.47752857
	Sptlc2	0.46808485
	Fn1	0.44640552
	Loxl2	0.44529066
	Klf2	0.44072027
*	S100a11	0.44052715
	Fbn1	0.42912497
	Ccnd2	0.42771652
	Cd63	0.42633846

gene	avg_logFC
Fchsd2	0.40561415
Klf4	0.40494123
Mmp2	0.39937238
Adgrg6	0.3928397
Col5a2	0.3788074
Vwf	0.36763662
Slit2	0.36753451
Vps4a	0.3669577
Pmp22	0.35555139
Clu	0.35219103
AU021092	0.34454944
Ptn	0.34017416
Nrp1	0.34008331
Htra1	0.33946908
Col26a1	0.33411637
Smpdl3a	0.33351794
Tmem120a	0.33328635
Gjc1	0.3307873
Alox12	0.32942225

Table S4. List of OG associated with genes in Supplementary table 3 The asterisks are the GO terms shown in Supplementary table 2.

	GO biological process complete	Fold Enrichment	raw P-value	FDR
	AV node cell to bundle of His cell communication by electrical coupling	> 100	0.0000320	0.01230
	cell communication by electrical coupling involved in cardiac conduction	> 100	0.0000480	0.01760
	regulation of retinal ganglion cell axon guidance	> 100	0.0000671	0.02200
	cellular response to laminar fluid shear stress	> 100	0.0000894	0.02710
	neural crest cell migration involved in autonomic nervous system develop	> 100	0.0001150	0.03060
	gap junction assembly	> 100	0.0001150	0.03010
	response to laminar fluid shear stress	> 100	0.0001150	0.02960
	neuron projection extension involved in neuron projection guidance	> 100	0.0001430	0.03530
	axon extension involved in axon guidance	> 100	0.0001430	0.03470
	cell communication by electrical coupling	> 100	0.0001430	0.03420
	actin-myosin filament sliding	> 100	0.0001750	0.03880
	dendrite arborization	> 100	0.0002100	0.04400
	AV node cell to bundle of His cell communication	99.95	0.0002480	0.04810
	positive regulation of nitric oxide biosynthetic process	35.09	0.0001020	0.02880
	positive regulation of nitric oxide metabolic process	34.36	0.0001090	0.03000
*	sprouting angiogenesis	28.43	0.0001860	0.04060
	positive regulation of reactive oxygen species biosynthetic process	26.6	0.0002240	0.04580
	endothelial cell migration	25.37	0.0002560	0.04860
	positive regulation of cell-substrate adhesion	16.53	0.0001100	0.02990
	cardiac chamber morphogenesis	15.59	0.0001370	0.03420
	positive regulation of chemotaxis	15.06	0.0001560	0.03610
	ameboidal-type cell migration	14.47	0.0000264	0.01120
	mesenchymal cell differentiation	13.92	0.0002100	0.04460
	negative regulation of neuron projection development	13.49	0.0002350	0.04630
	regulation of endothelial cell migration	13.01	0.0002690	0.04990
	heart morphogenesis	12.45	0.0000089	0.00517
	regulation of cell-substrate adhesion	12.44	0.0000534	0.01870
	extracellular matrix organization	12.31	0.0000094	0.00531
	external encapsulating structure organization	12.26	0.0000096	0.00523
	extracellular structure organization	12.26	0.0000096	0.00506
	regulation of epithelial cell migration	11.55	0.0000753	0.02370
*	angiogenesis	10.15	0.0000274	0.01110
	negative regulation of locomotion	9.96	0.0000304	0.01190
	heart development	9.73	0.0000001	0.00013
	negative regulation of cell migration	9.71	0.0001670	0.03810
	negative regulation of cell motility	9.29	0.0002050	0.04420
	negative regulation of cellular component movement	9.01	0.0002350	0.04680
*	blood vessel morphogenesis	8.77	0.0000139	0.00685
	positive regulation of cell adhesion	8.73	0.0000143	0.00684
	blood circulation	8.01	0.0001000	0.02920
	regulation of anatomical structure size	7.72	0.0000079	0.00494
	regulation of cell adhesion	7.5	0.0000006	0.00064
	circulatory system process	7.45	0.0001480	0.03480

*	blood vessel development	7.11	0.0000519	0.01860
	regulation of neuron projection development	7.05	0.0000549	0.01880
*	vasculature development	6.74	0.0000726	0.02330
	circulatory system development	6.55	0.0000006	0.00063
	positive regulation of locomotion	6.39	0.0001010	0.02880
	tissue morphogenesis	6.16	0.0001270	0.03220
	negative regulation of multicellular organismal process	6.07	0.0000003	0.00045
	tissue development	5.91	0.0000000	0.00000
	cell adhesion	5.85	0.0000177	0.00821
	regulation of cell migration	5.85	0.0000055	0.00378
	biological adhesion	5.78	0.0000194	0.00851
	regulation of cell motility	5.55	0.0000087	0.00526
	regulation of response to external stimulus	5.54	0.0000271	0.01120
	regulation of locomotion	5.3	0.0000131	0.00664
*	anatomical structure formation involved in morphogenesis	5.22	0.0000427	0.01600
	regulation of cellular component movement	5.11	0.0000178	0.00801
	cell migration	4.97	0.0001700	0.03820
	regulation of apoptotic process	4.87	0.0000012	0.00103
	animal organ morphogenesis	4.81	0.0000807	0.02490
	negative regulation of apoptotic process	4.77	0.0002240	0.04530
	regulation of programmed cell death	4.75	0.0000015	0.00122
	epithelium development	4.73	0.0000914	0.02720
	negative regulation of programmed cell death	4.67	0.0002610	0.04900
	regulation of cell population proliferation	4.55	0.0000009	0.00088
	animal organ development	4.37	0.0000000	0.00000
	regulation of cell death	4.29	0.0000048	0.00360
*	anatomical structure morphogenesis	4.13	0.0000001	0.00023
	movement of cell or subcellular component	3.78	0.0002190	0.04550
	cell development	3.64	0.0000617	0.02070
	regulation of multicellular organismal process	3.55	0.0000005	0.00062
	system development	3.29	0.0000000	0.00001
	cell differentiation	3.24	0.0000001	0.00025
	cellular developmental process	3.2	0.0000002	0.00026
	multicellular organism development	2.99	0.0000000	0.00001
	anatomical structure development	2.98	0.0000000	0.00000
	developmental process	2.87	0.0000000	0.00000
	negative regulation of cellular process	2.62	0.0000012	0.00107
	negative regulation of biological process	2.4	0.0000058	0.00382
	positive regulation of cellular process	2.33	0.0000052	0.00375
	positive regulation of biological process	2.32	0.0000013	0.00108
	multicellular organismal process	2.25	0.0000001	0.00017
*	cellular component organization	2.13	0.0002540	0.04880